Numerical modelling of the strain localization in soils and rocks

Collin F., Levasseur S., B. Pardoen, F. Salehnia

R. Chambon, D. Caillerie, P. Bésuelle

P. Kotronis, G. Jouan, M. Soufflet

First International Workshop on the Finite Element Code LAGAMINE
(LAGASHOP 2013)
9-12 September 2013
University of Liège, Opera Complex, Liège

Failure in soils and rocks is almost always associated with fractures and/or shear bands developing in the geomaterial.

Shear banding occurs frequently (at many scales) and is the source of many soil and rock engineering problems:

natural or human-made slopes or excavations, unstable rock masses, embankments or dams, tunnels and mine galleries, boreholes driven for oil production, repositories for nuclear waste disposal

In geomaterials, the understanding of failure processes is more complex by the fact that soils and rocks are multiphase porous materials where different multiphysical processes take place.

In situ observations of shear banding and/or faulting are made frequently at many scales

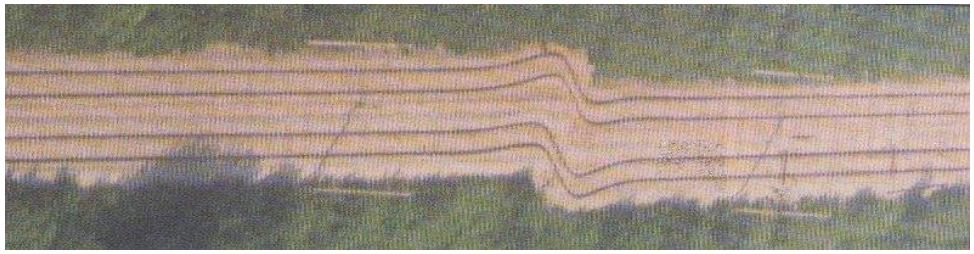

Large scale: railway tracks after an earthquake in Turkey

In situ observation of shear banding

Human-made slope along E42 exit road

Bierset (Belgium) 1998 – Courtesy C. Schroeder

Nuclear waste disposal

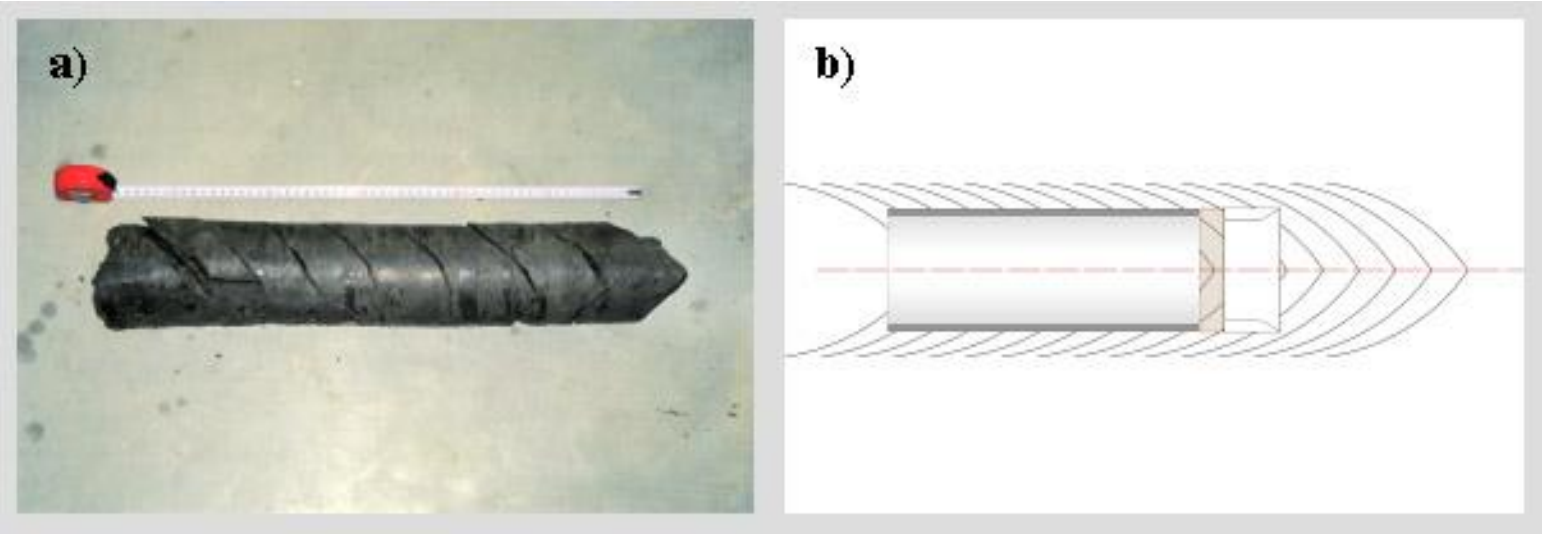

Fractures observed during the construction of the connecting gallery at the URL in Mol. Vertical cross section through the gallery showing the fracturation pattern around it, as deduced from the observations (from Alheid et al. 2005)

Outline:

- *Introduction*
- *Experimental observations*
- *Theoretical tools*
- *Numerical models*
- *Conclusions*

To better understand the development of the shear band, experiments are necessary, which are no more element tests as far as the behavior becomes heterogeneous.

- Biaxial test
- Axisymetric triaxial test
- True triaxial test

Different teams have performed experimental works devoted to the study of strain localization:

- Desrues and co-workers
- Finno and co-workers
- Vardoulakis and co-workers
- …

Triaxial test:

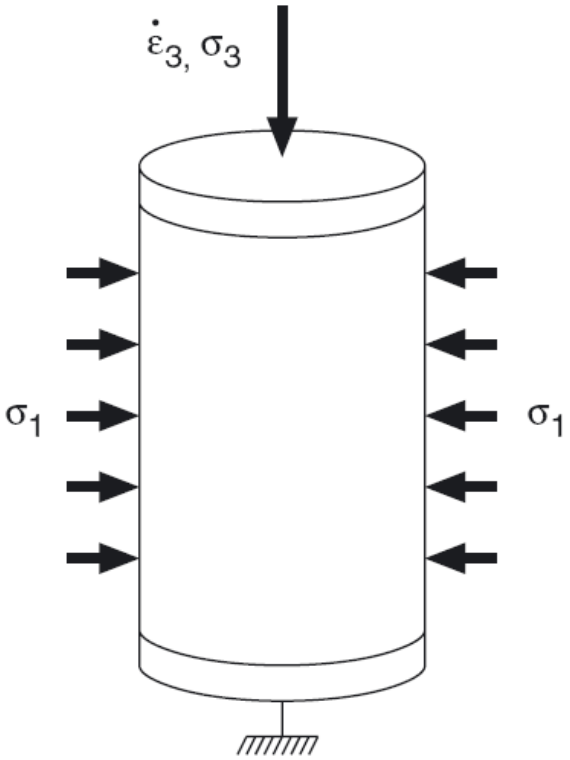

In triaxial tests (and more generally in axi-symmetric tests), the localization zone may remain more or less hidden inside the sample (need for special techniques to see the process)

Experimental observations: triaxial test

Localized rupture in sandstone samples under different confining pressures (Bésuelle et al., 2000)

Experimental characterisation of the localisation phenomenon inside a Vosges sandstone in a triaxial cell
P. BESUELLE, J. DESRUES, S. RAYNAUD, International Journal of Rock Mechanics & Mining Sciences 37 (2000) p. 1223-1237

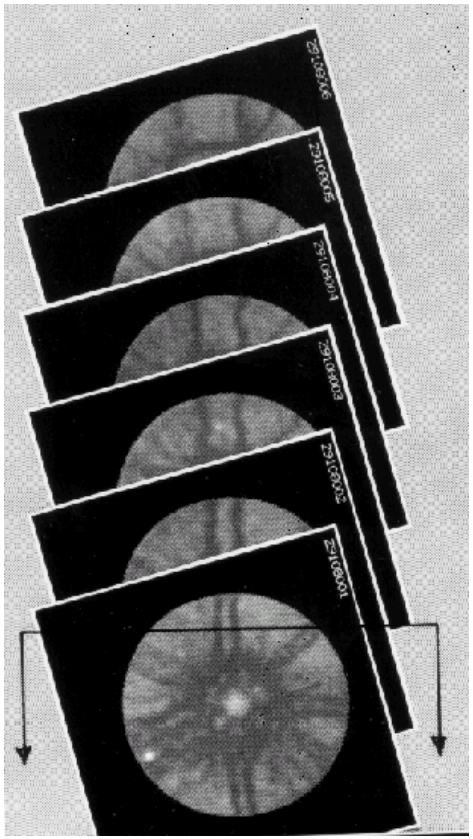

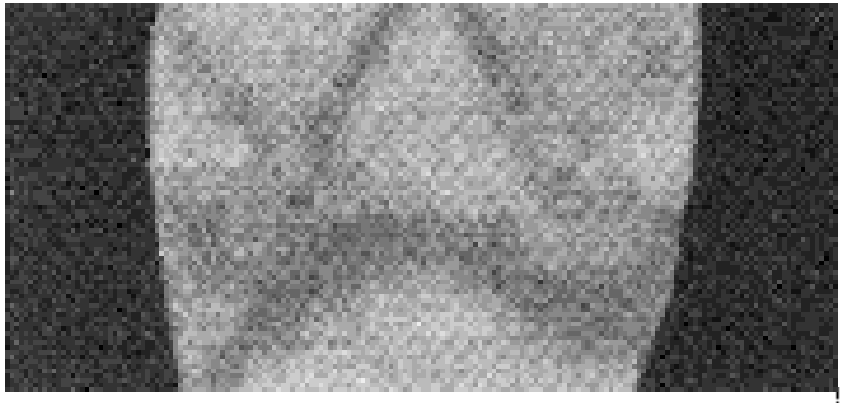

Tomodensitometry:

Localization pattern observed in sand sample during axisymetric triaxial test

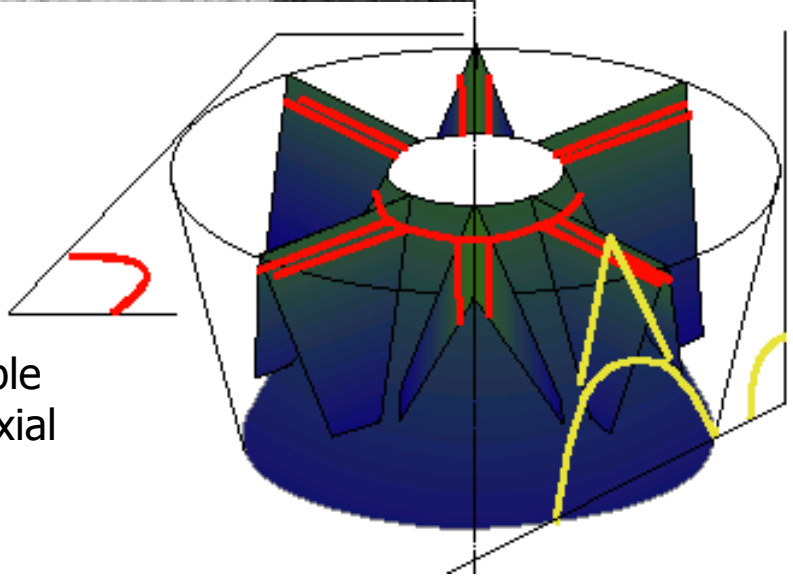

Desrues, J. *et al.* (1996). Géotechnique 46, No. 3, 529–546

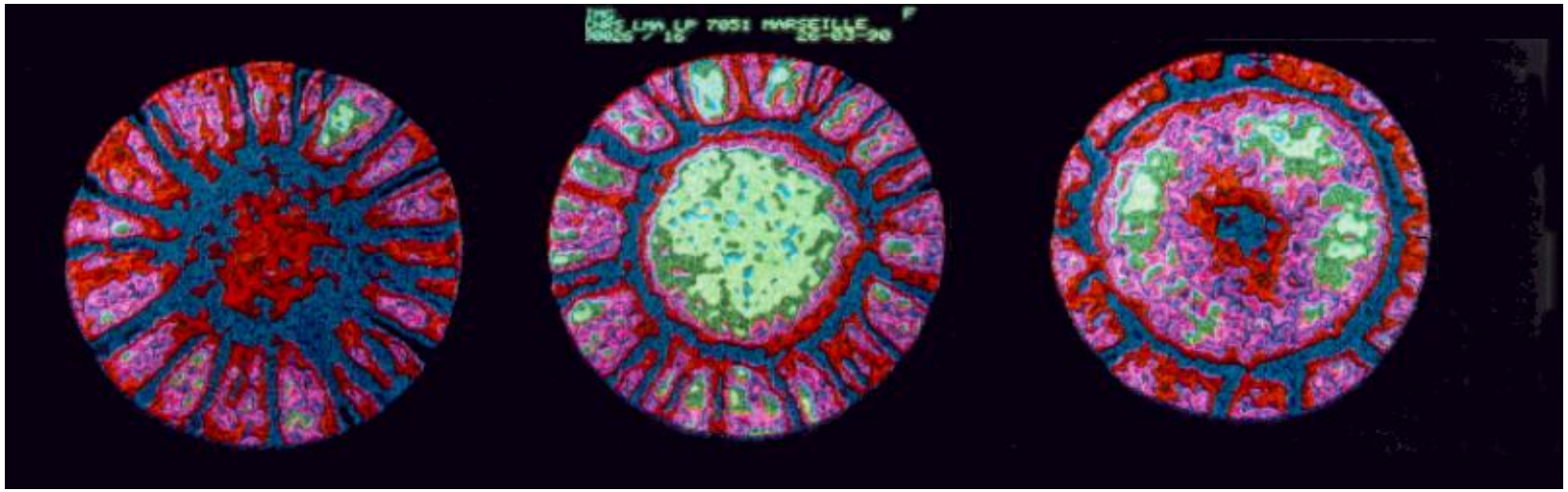

Tomodensitometry:

Localization pattern observed in sand sample during axisymetric triaxial test

Experimental observations: triaxial test

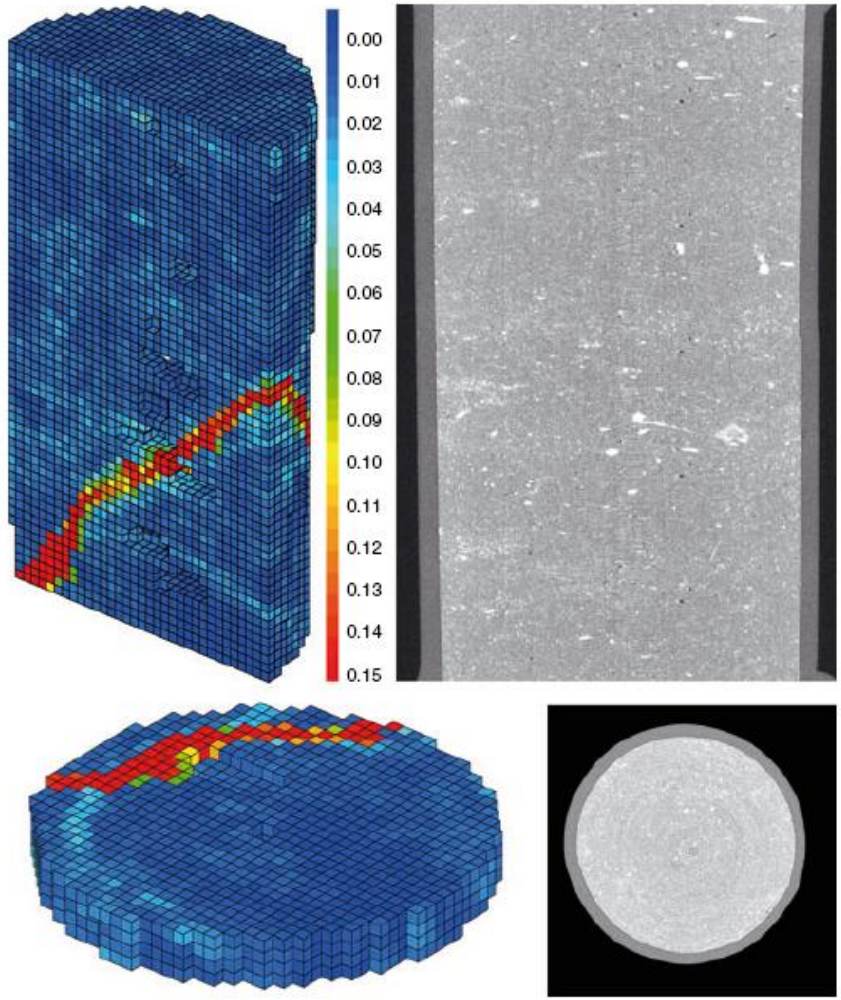

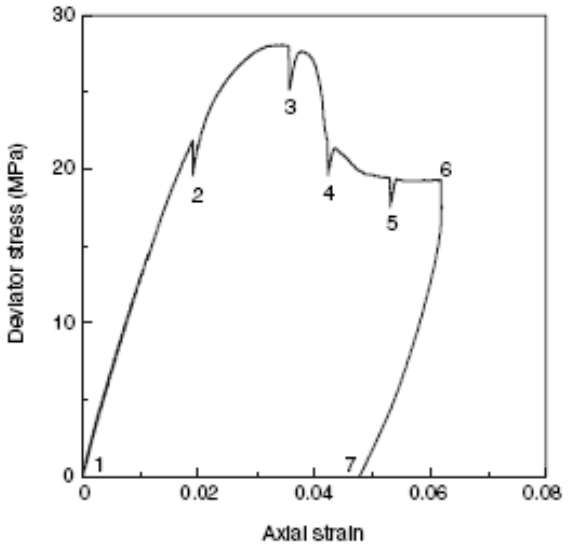

Figure 6: Deviator stress versus axial strain response recorded during test *ES1SYN01* (10 MPa confining stress)

Increment 4-5

3D digital image correlation applied to X-ray micro tomography images from triaxial compression tests on argillaceous rock *LENOIR N , Bornert M, DESRUES J, BESUELLE P, VIGGIANI G Strain* vol:43 No 3 pp.193-205

Biaxial test:

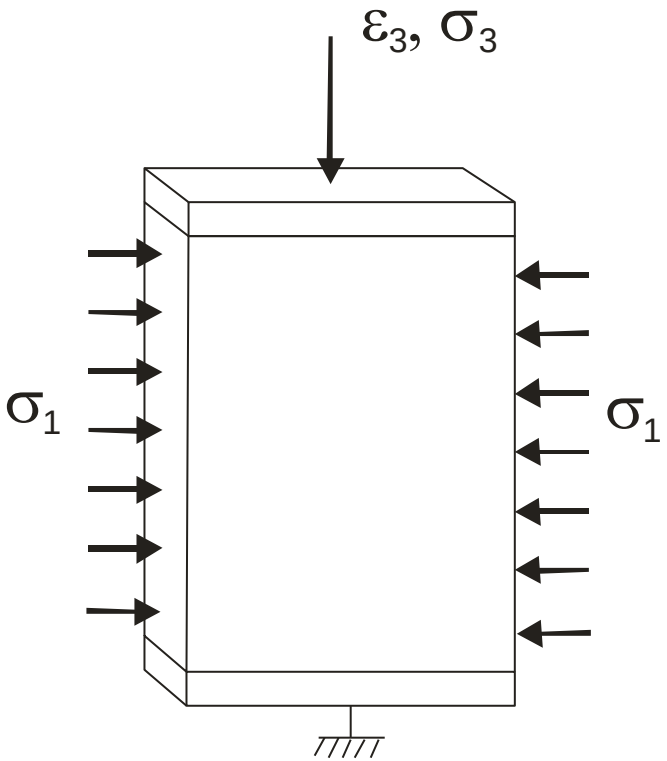

As in triaxial tests (and more generally in axi-symmetric tests), the localization zone may remain more or less hidden inside the sample, most of the experimental campaigns on localization have been performed in biaxial apparatus

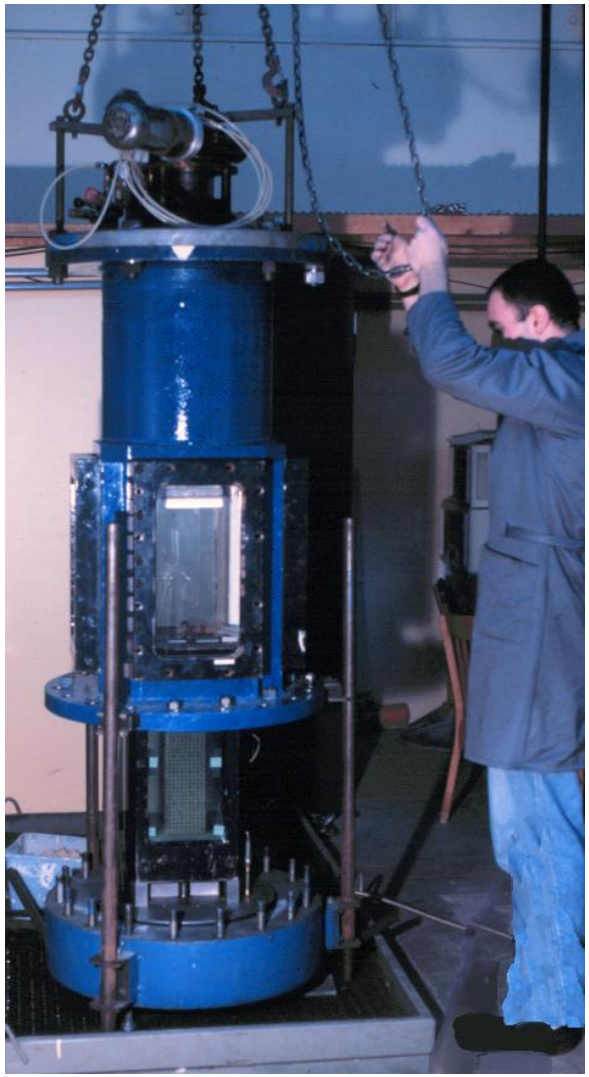

Experimental
set-up
&
a typical test

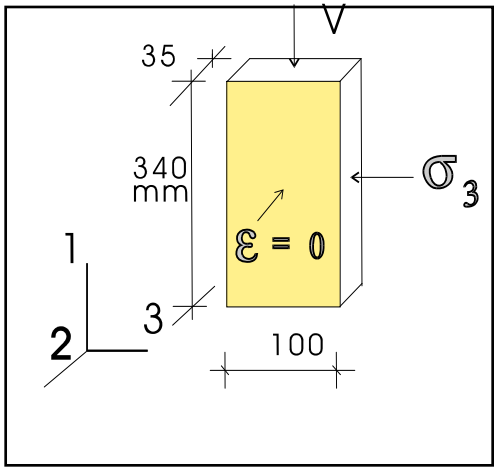

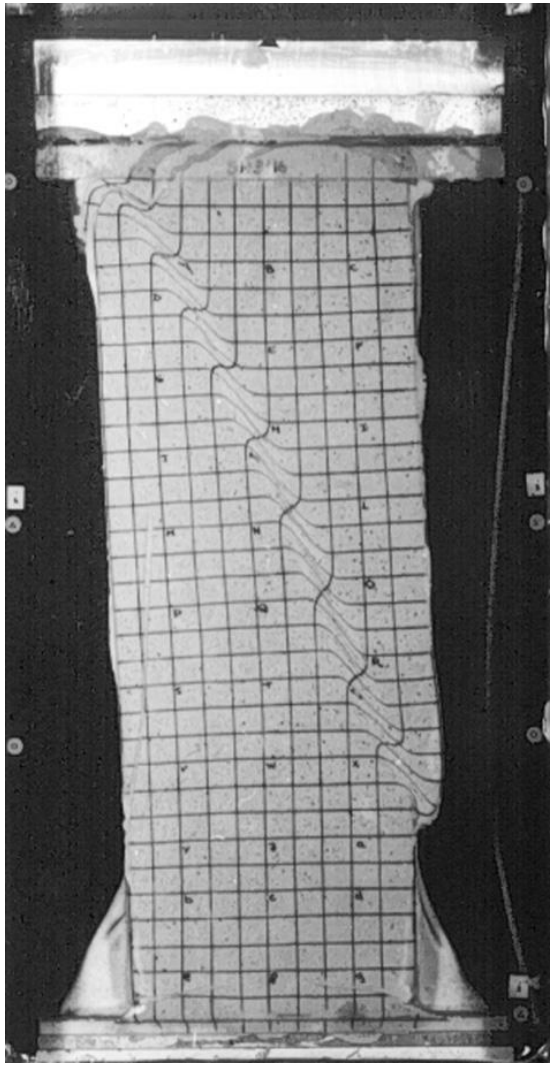

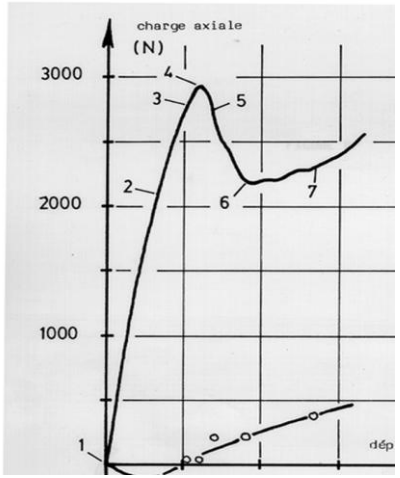

Localization and Peak

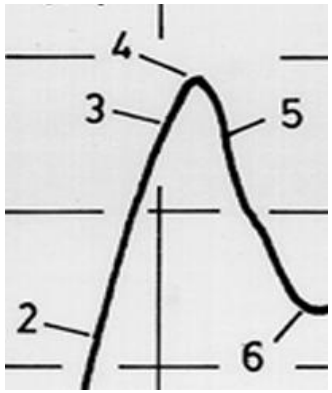

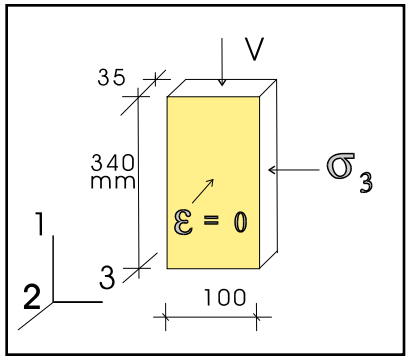

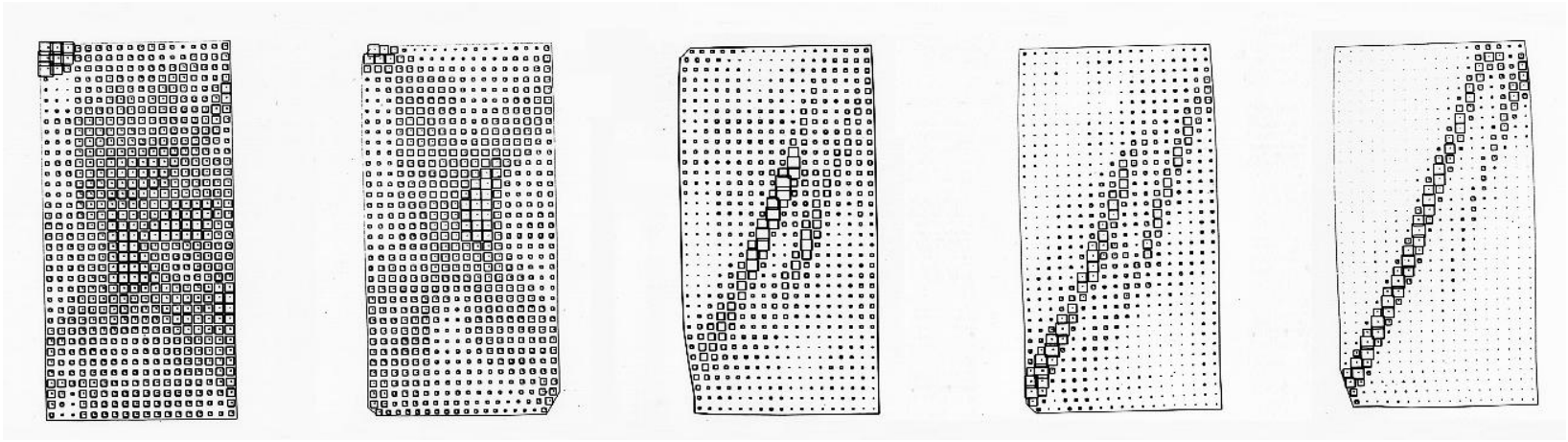

1-2 2-3 3-4 4-5 5-6

Outline:

- *Introduction*
- *Experimental observations*
- *Theoretical tools*
- *Numerical models*
- *Conclusions*

Experimental evidence:

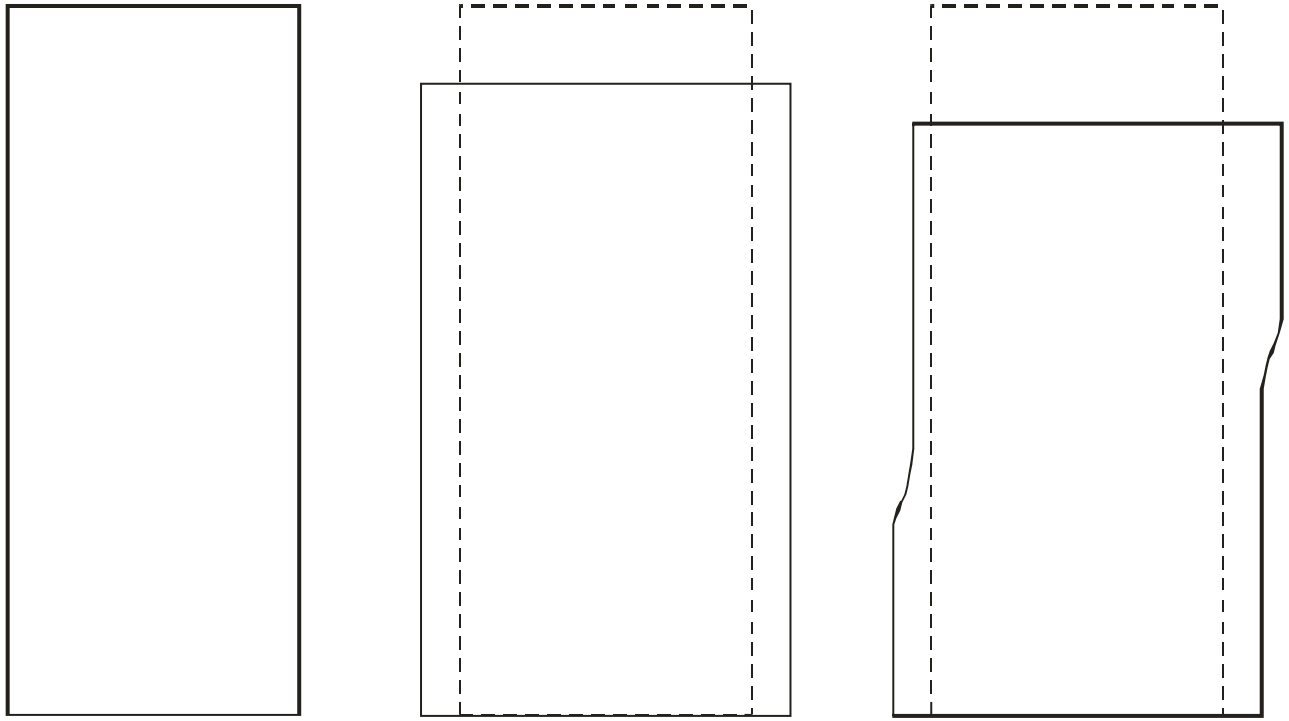

Initial state

Homogeneous strain field

Localized strain field

Theoretical background

Following the previous works by (Hadamard, 1903), (Hill, 1958) and (Mandel, 1966), Rice and co-workers (Rice, 1976, Rudnicki et al., 1975) have proposed the so-called Rice criterion.

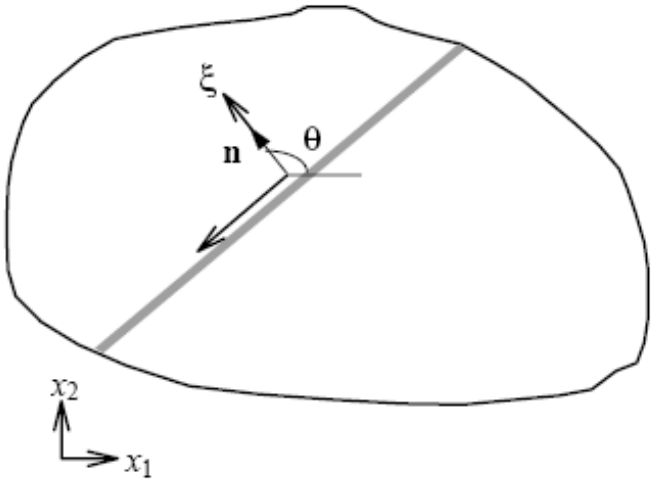

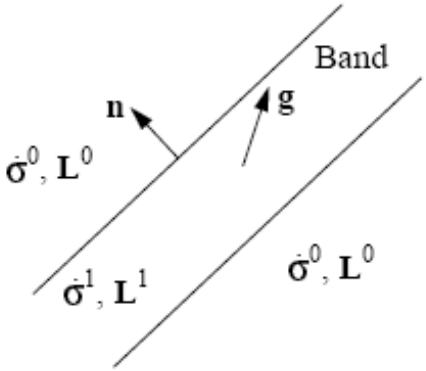

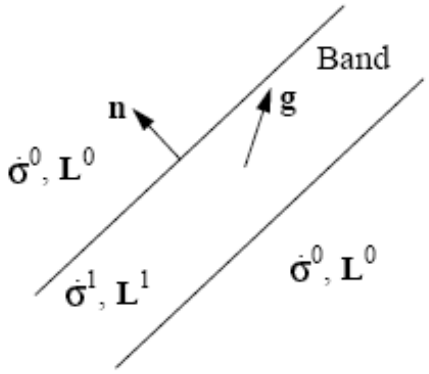

Static condition: $n\left(\dot{\sigma}^1 - \dot{\sigma}^0\right) = 0$

Kinematic condition: $L^1 = L^0 + \Delta L$

$$L^1 = L^0 + g \otimes n$$

$$L = \frac{1}{2}\left(\frac{\partial \dot{u}_i}{\partial x_j} + \frac{\partial \dot{u}_j}{\partial x_i}\right)$$

Constitutive law: $\dot{\sigma} = C : L$

$$n\left(C^1 : (L^0 + g \otimes n) - C^0 : L^0\right) = 0$$

When it is assumed that $C^1 = C^0 = C$, no trivial solution if and only if:

$$\det(nCn) \leq 0$$

Constitutive law in principal axis:

$$\begin{Bmatrix} \dot{\sigma}_{11} \\ \dot{\sigma}_{22} \\ \dot{\sigma}_{12} \end{Bmatrix} = \begin{bmatrix} C_{11} & C_{12} & 0 \\ C_{21} & C_{22} & 0 \\ 0 & 0 & 2G_{12} \end{bmatrix} \begin{Bmatrix} L_{11} \\ L_{22} \\ L_{12} \end{Bmatrix}$$

Static condition:

$$\left(\dot{\sigma}_{ij}^{1} - \dot{\sigma}_{ij}^{0}\right) n_j = 0$$

$$\begin{cases} \left(\dot{\sigma}_{11}^{1} - \dot{\sigma}_{11}^{0}\right) n_1 + \left(\dot{\sigma}_{12}^{1} - \dot{\sigma}_{12}^{0}\right) n_2 = 0 \\ \left(\dot{\sigma}_{21}^{1} - \dot{\sigma}_{21}^{0}\right) n_1 + \left(\dot{\sigma}_{22}^{1} - \dot{\sigma}_{22}^{0}\right) n_2 = 0 \end{cases}$$

Kinematic condition:

$$L_{ij}^{1} = L_{ij}^{0} + g_i n_j$$

Combining the three previous relationship yields:

If $C^1 = C^0 = C$:

$$\begin{cases} \left(C_{11} g_1 n_1 + C_{12} g_2 n_2\right) n_1 + G_{12}\left(g_1 n_2 + g_2 n_1\right) n_2 = 0 \\ G_{12}\left(g_1 n_2 + g_2 n_1\right) n_1 + \left(C_{21} g_1 n_1 + C_{22} g_2 n_2\right) n_2 = 0 \end{cases}$$

$$\begin{cases} \left(C_{11}n_1^{\,2} + G_{12}n_2^{\,2}\right)g_1 + \left(C_{12}n_1n_2 + G_{12}n_2n_1\right)g_2 = 0 \\ \left(C_{21}n_1n_2 + G_{12}n_2n_1\right)g_1 + \left(C_{22}n_2^{\,2} + G_{12}n_1^{\,2}\right)g_2 = 0 \end{cases}$$

When it is assumed that $C^1 = C^0 = C$, no trivial solution if and only if: $\det(nCn) \le 0$

$$\left(C_{11}G_{12}\right)n_1^{\,4} + \left(C_{22}G_{12}\right)n_2^{\,4} + \left(C_{11}C_{22} - 2C_{12}G_{12} - C_{12}^2\right)n_1^{\,2}n_2^{\,2} = 0$$

$$n_1^{\,4}\left(a_1\,z^4 + a_3\,z^2 + a_5\right) = 0 \qquad z = \frac{n_2}{n_1}$$

For a constitutive law written in cartesian axis:

$$n_1^{\,4}\left(a_1\,z^4 + a_2\,z^3 + a_3\,z^2 + a_4\,z + a_5\right) = 0$$

Extension to multiphysical context, mainly in hydro mechanical coupling:

Loret and co-workers (Loret et al., 1991) showed that for hydromechanical problems the condition of localization depends only on the **drained properties** of the medium

In coupled problems much more **complex localization pattern** can be obtained, at least theoretically (Vardoulakis, 1996)

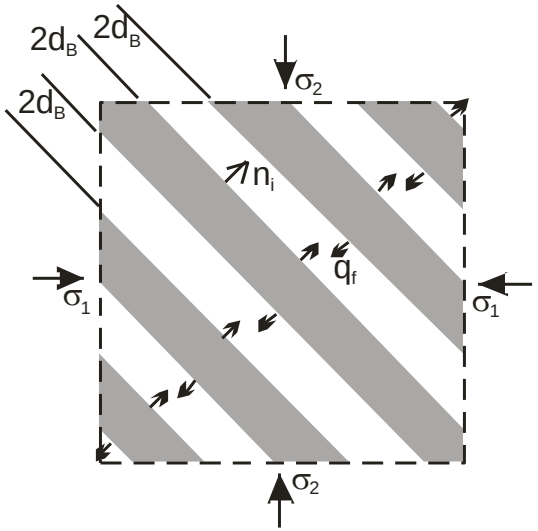

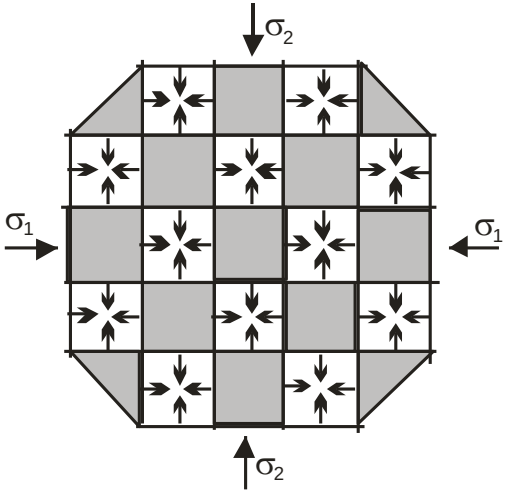

Which information can provide these theoretical tools ?

For element test, the tools allow you to check if and when the constitutive model is able to predict the localization direction observed at the laboratory.

For boundary value problems, they provide you the stress state when bifucation may arise and the direction of potential bifurcation (fracturation). Be aware that the Rice criterion is a local one !

This criterion could be activated for any constitutive model, if you make the connection in the ELEMB2 and POSPEC routines and some additional state variables have to be defined.

Skeleton mechanical behaviour

Linear elasticity : E_0 *et* ν_0

Drucker Prager criterion :

$$F \equiv \sqrt{\frac{3}{2}} II_{\hat{\sigma}} + m\left(I_\sigma - \frac{3c}{\tan\phi} \right) = 0$$

$$m = \frac{2\sin\phi}{3-\sin\phi} \qquad c = c_0\, f(\gamma^p)$$

Associated softening plasticity (decrease of cohesion) :

$$f(\gamma^p) = \left(1-(1-\alpha)\frac{\gamma^p}{\gamma_R^p} \right)^2 \; si \; 0 < \gamma^p < \gamma_R^p$$

$$= \alpha^2 \; si \; \gamma^p \geq \gamma_R^p$$

Softening behaviour : localization effects are very important

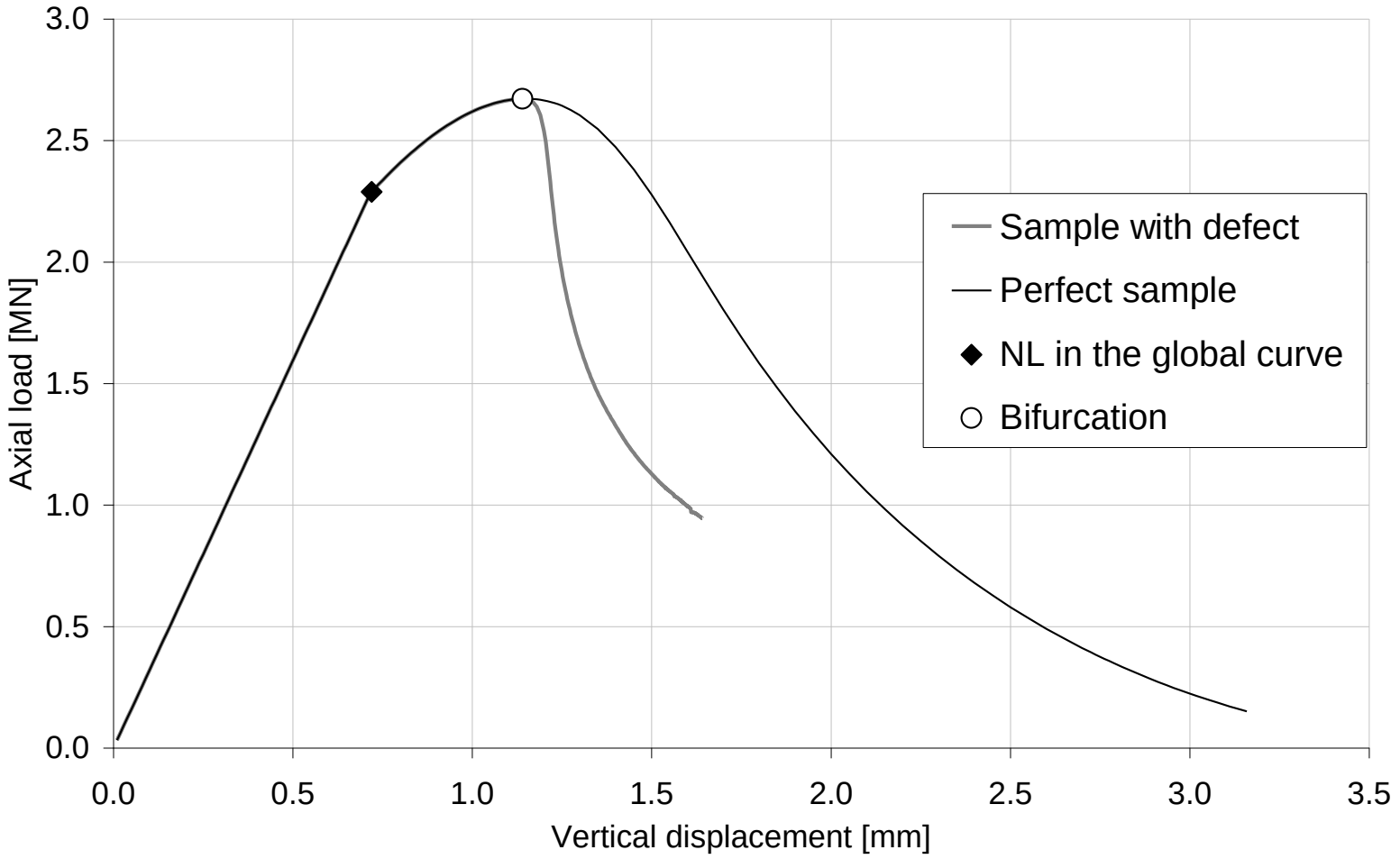

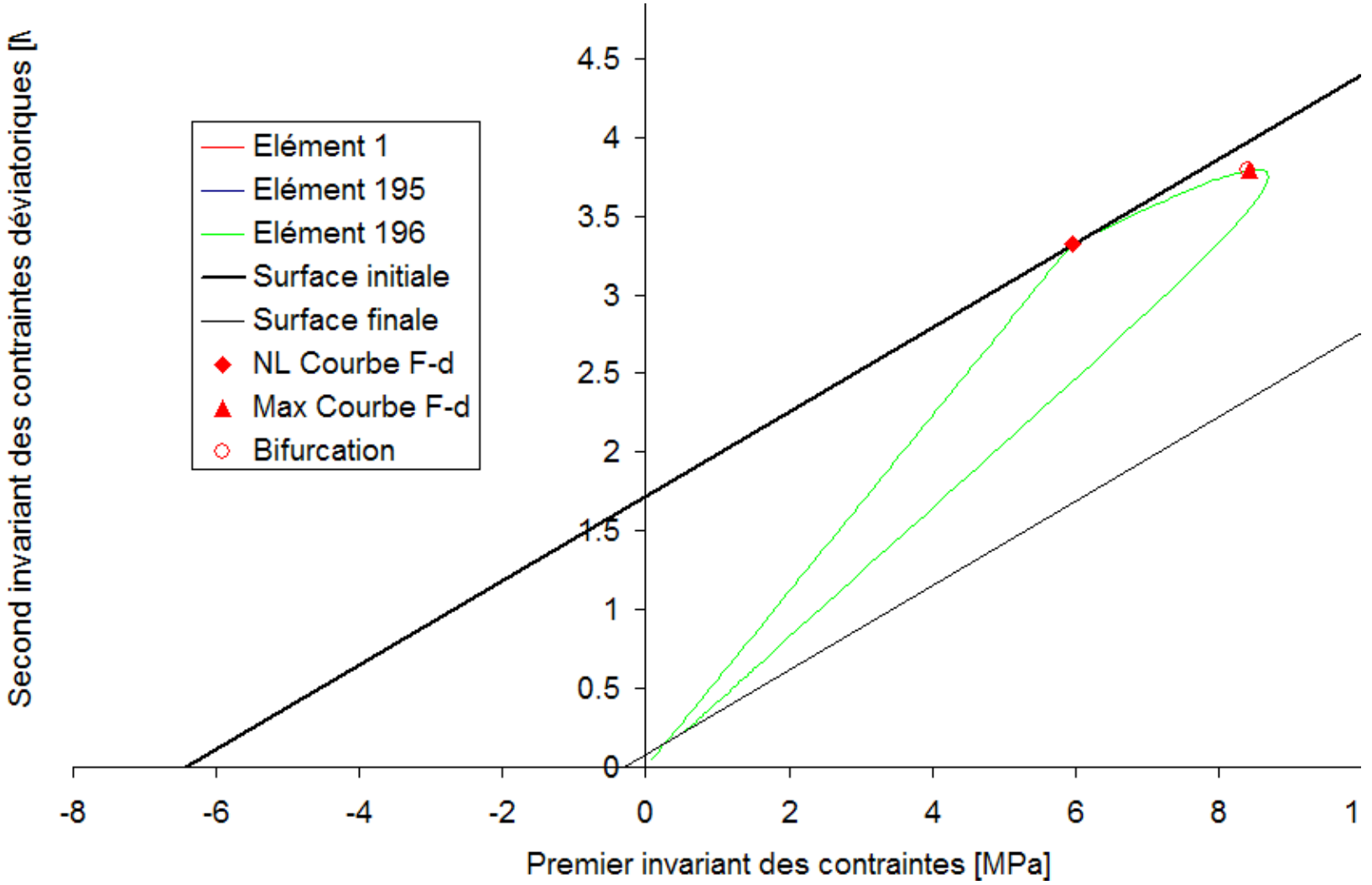
Second invariant des contraintes déviatoriques [M
Premier invariant des contraintes [MPa]
Elément 1
Elément 195
Elément 196
Surface initiale
Surface finale
NL Courbe F-d
Max Courbe F-d
Bifurcation
4.5
4
3.5
3
2.5
2
1.5
1
0.5
0
-8
-6
-4
-2
0
2
4
6
8
1

Softening behaviour : localization effects are very important

Bifurcation analysis thanks to the Rice criterion (Acoustic tensor)

$$\det\left(\underline{\Lambda}(\vec{n})\right) = n_1^4 \left(a_1 z^4 + a_2 z^3 + a_3 z^2 + a_4 z + a_5\right) \leq 0$$

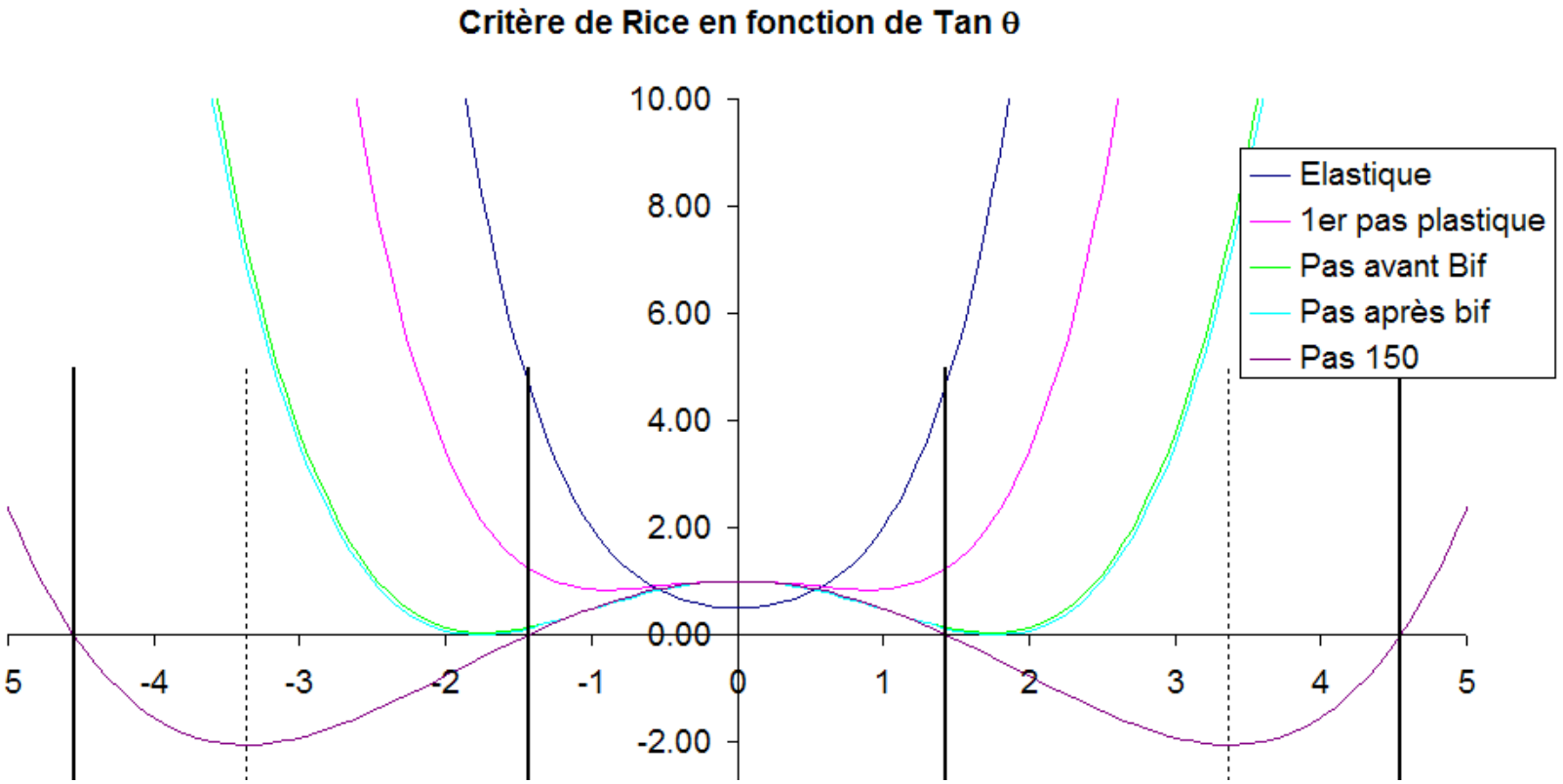

Plastic point

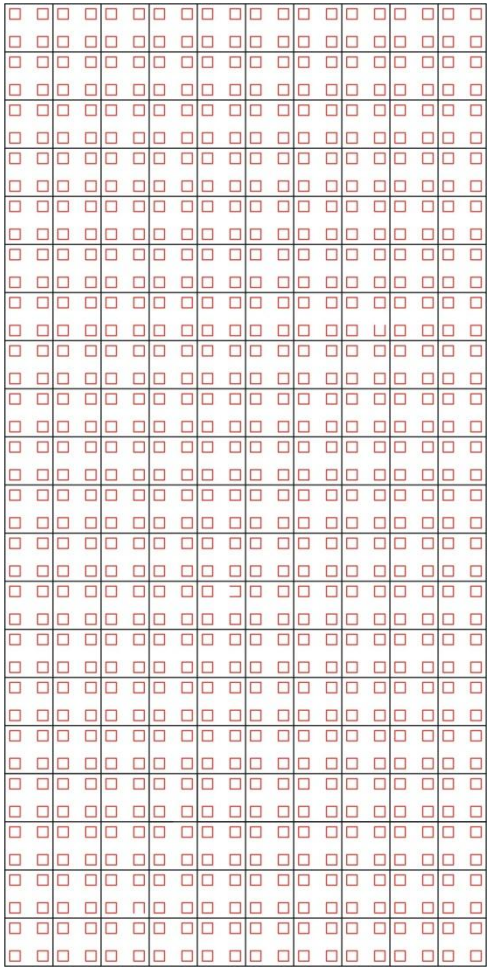

Bifurcation dir.

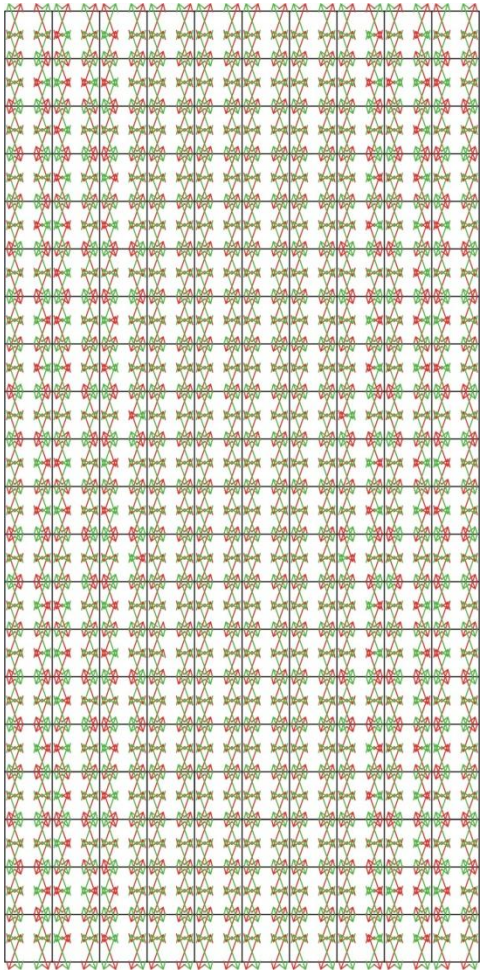

Bifurcation cones

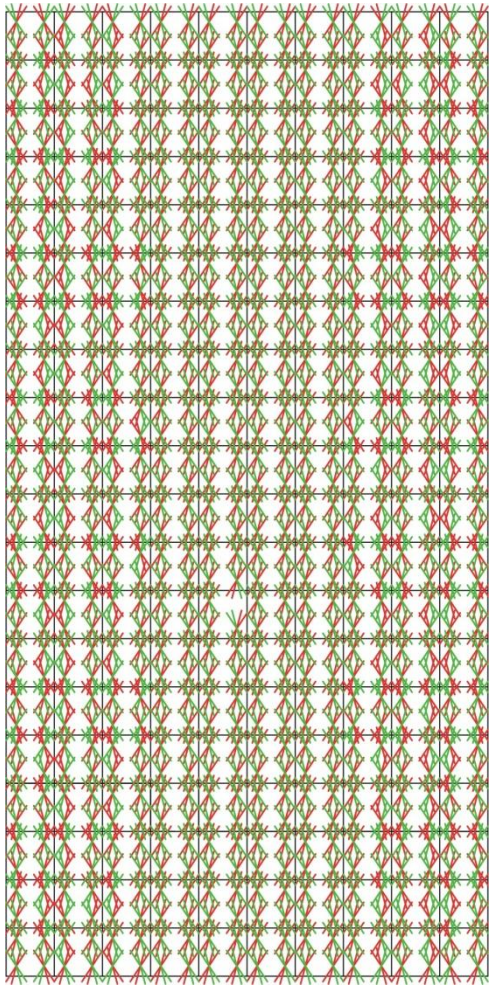

Plastic point *Bifurcation dir.* *Bifurcation cones*

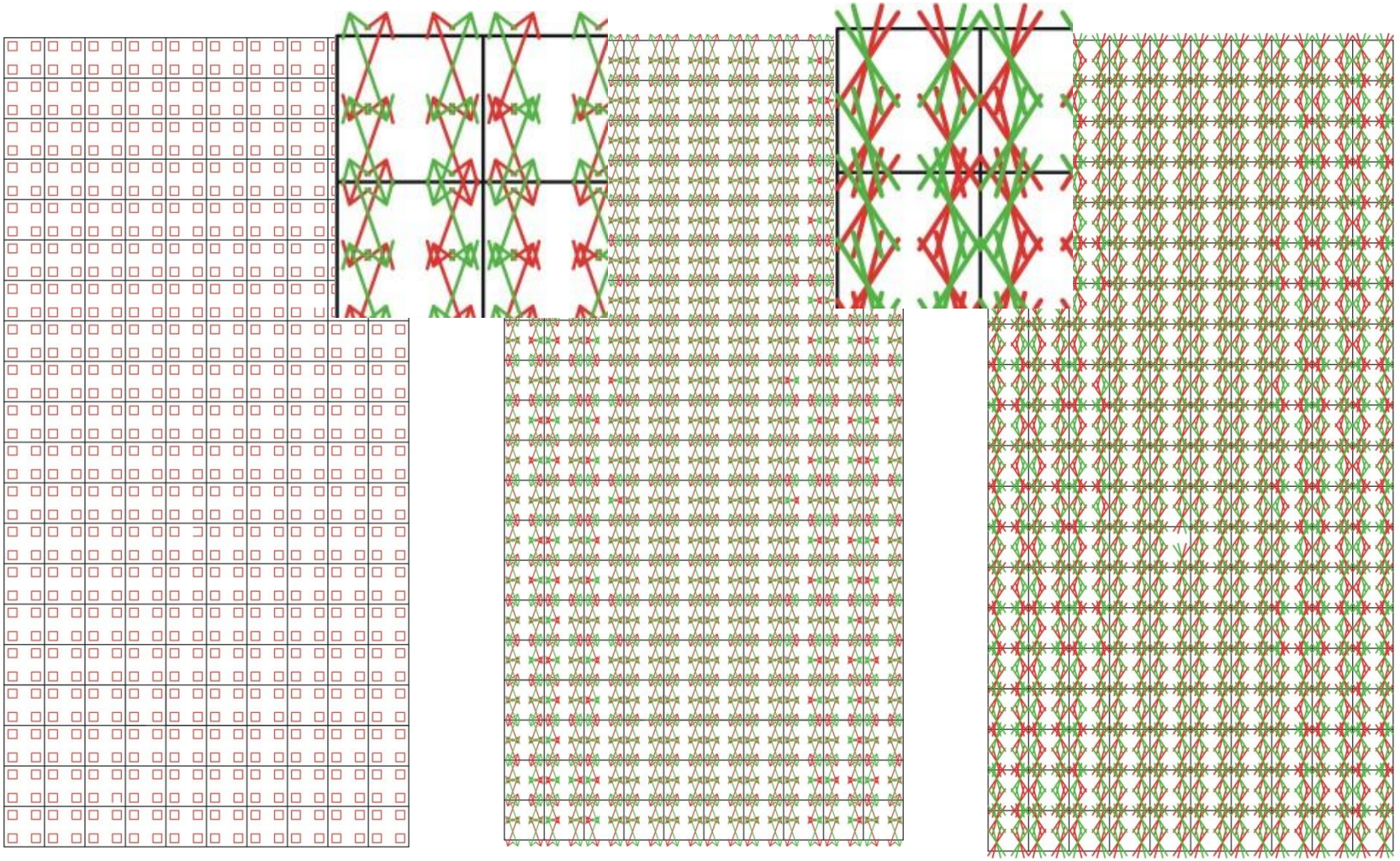

The Rice criterion provides us the information on when and how localization may appear.
Do we have any problem to model such phenomenon with classical finite element method ?

Let's consider the modelling of a biaxial with a defect triggering the localization, first without any hydromechanical effect.

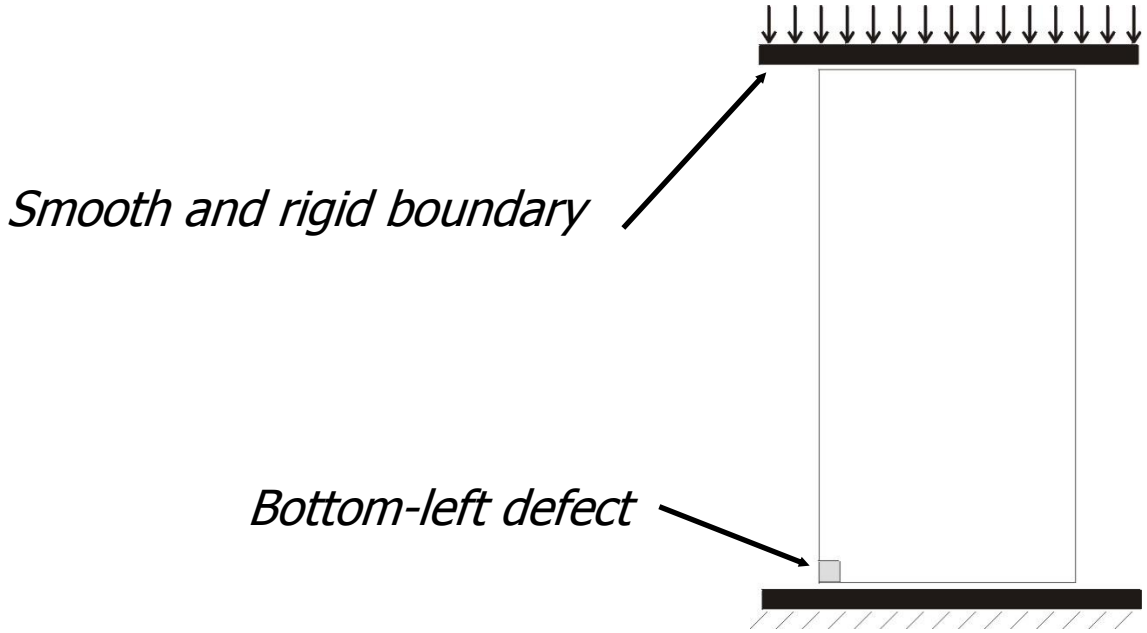

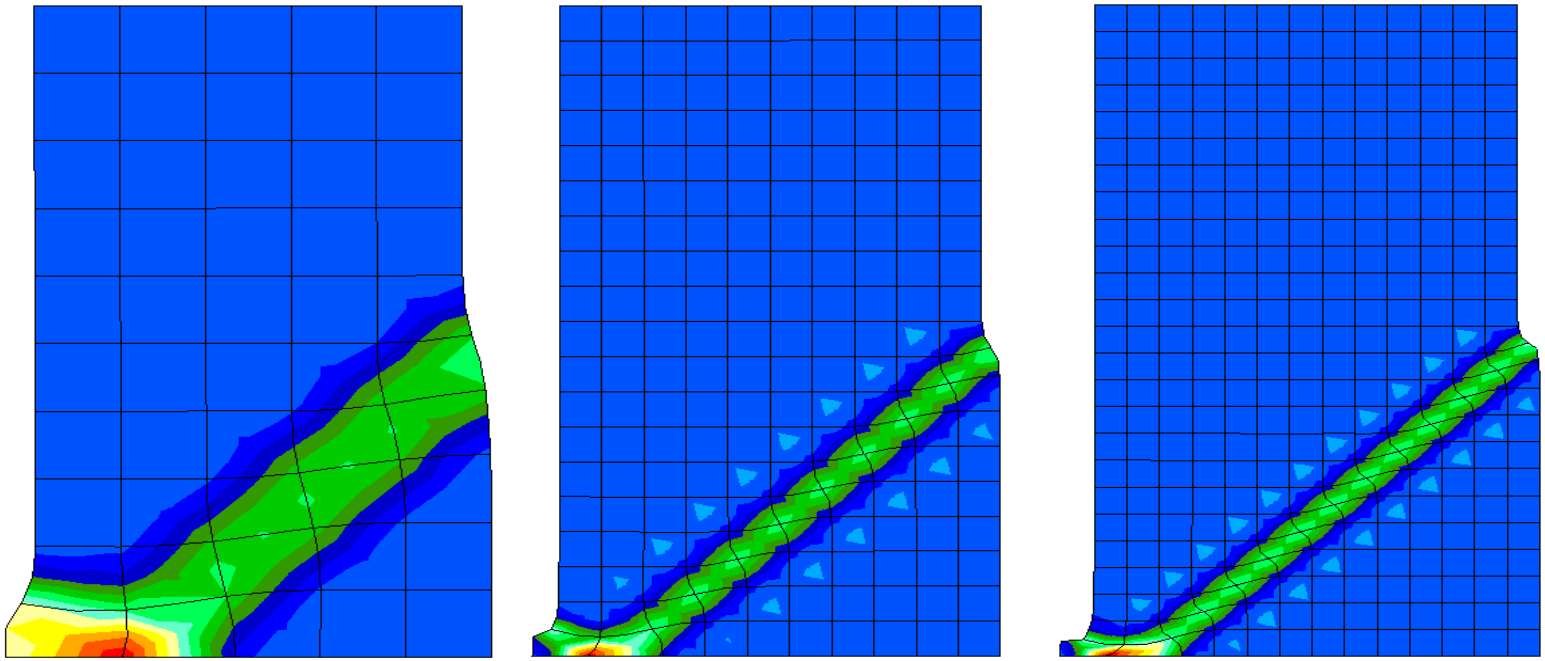

50 elements

200 elements

300 elements

The post peak behaviour depends on the mesh size !

Let's consider now a coupled modelling:

Cylindrical cavity without retaining

Anisotropic initial state of stress

Geometrical dimensions : *Internal radius 3 m*

Mesh length 60 m

Choice :

Symetry of the problem is assumed

894 elements – 2647 nodes – 7941 dof

Example of EDZ around a cavity

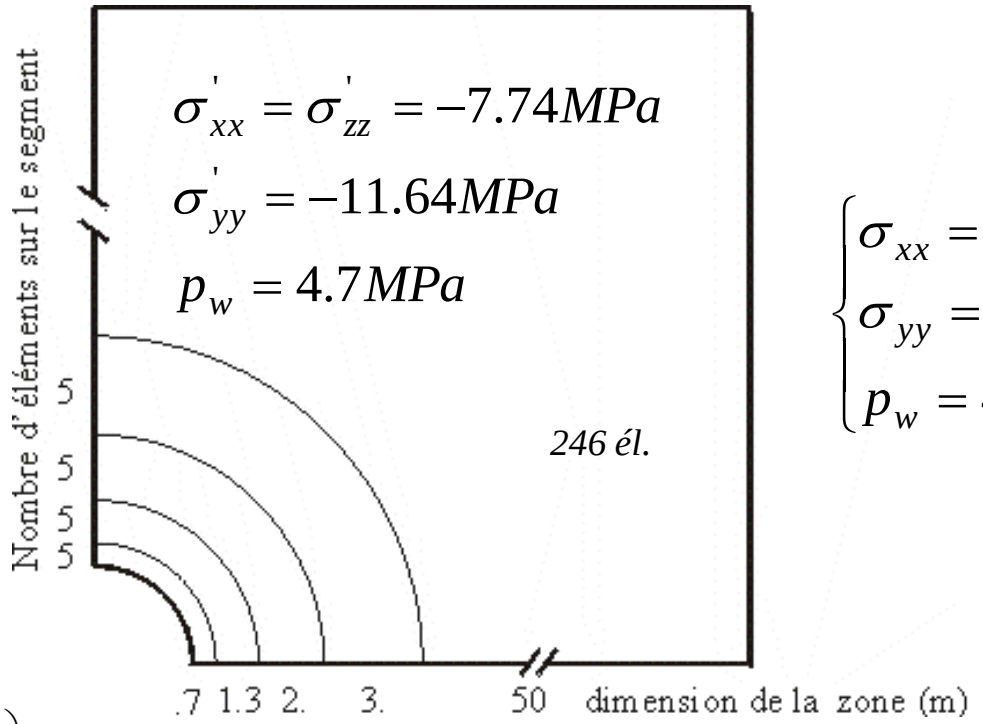

$$\begin{cases} \sigma_{xx} = -11.5MPa \\ \sigma_{yy} = -15.4MPa \\ p_w = 4.7MPa \end{cases}$$

$$\begin{cases} 0 \le t \le T \\ \sigma_{xx} = \sigma'_{xx} - bS_{rw}p_w = -11.5\left(1 - \frac{t}{T}\right)MPa \\ \sigma_{yy} = \sigma'_{yy} - bS_{rw}p_w = -15.4\left(1 - \frac{t}{T}\right)MPa \\ p_w = 4.7\left(1 - \frac{t}{T}\right)MPa \\ t > T \\ \sigma_{xx} = \sigma_{yy} = p_w = 0 \end{cases}$$

T = 1.5 Ms (17 jours)

t_{total} = 300 Ms (9.5 ans)

Coupled modelling – Comparison Coarse mesh / Refined mesh

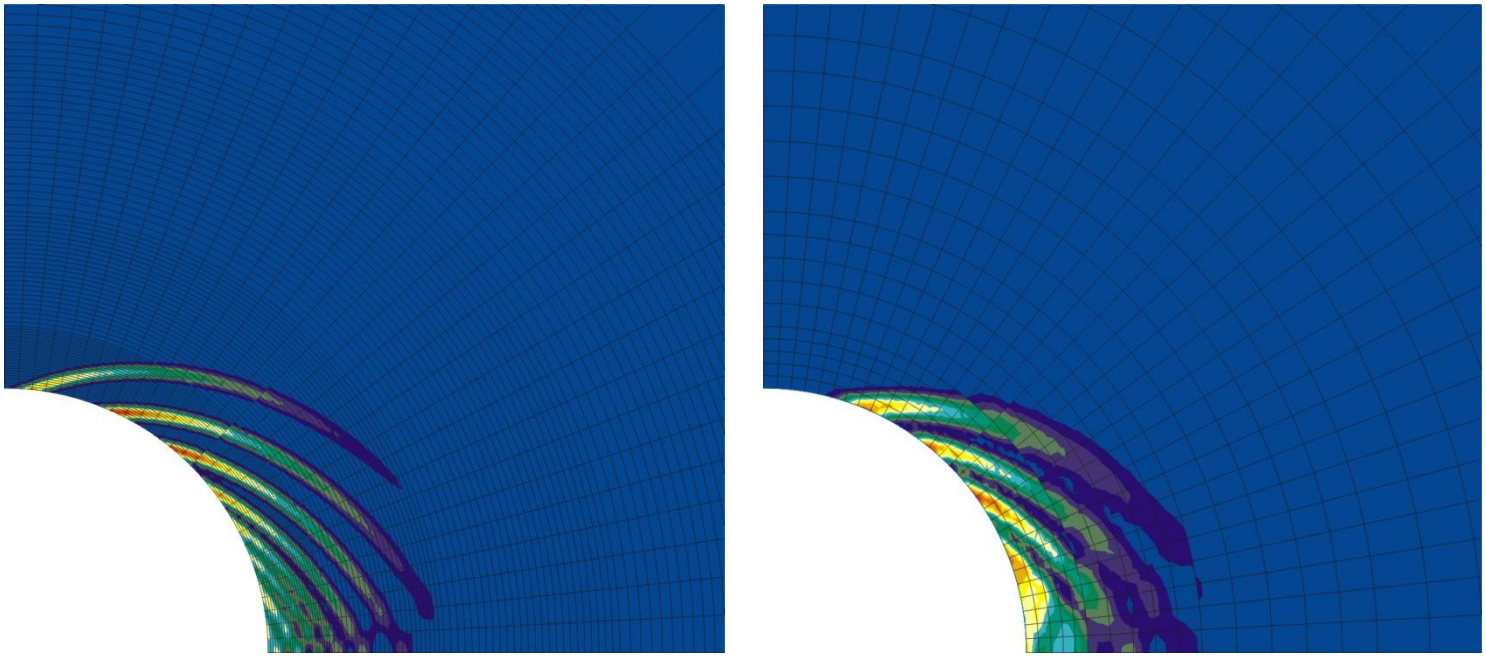

Deviatoric strains

- Localization study : Acoustic tensor determinent
- Mesh dependency of the results for classical FE
- Non-uniqueness of the results in both cases

The numerical modelling of strain localization with classical FE is not adequate.

We need another numerical model to fix this mesh dependency problem !

Outline:

- *Introduction*
- *Experimental observations*
- *Theoretical tools*
- *Numerical models*
- *Conclusions*

- Classical FE formulation: mesh dependency
- Different regularization methods

Gradient plasticity

Enrichment of the law

Non-local approach

Microstructure continuum

Cosserat model

Enrichment of the kinematics

Second gradient local model

Mainly for monophasic materials !

In second gradient model, the continuum is enriched with microstructure effects. The kinematics include therefore the classical one but also microkinematics (See Germain 1973, Toupin 1962, Mindlin 1964).

Let us define first the classical kinematics:

- u_i is the (macro) displacement field
- F_{ij} is the macro displacement gradient which means:

$$F_{ij} = \frac{\partial u_i}{\partial x_j}$$

- D_{ij} is the macro strain:

$$D_{ij} = \frac{1}{2}(F_{ij} + F_{ji})$$

- R_{ij} is the macro rotation:

$$R_{ij} = \frac{1}{2}(F_{ij} - F_{ji})$$

Here is the enrichment:

- f_{ij} is the microkinematic gradient.
- d_{ij} is the microstrain:

$$d_{ij} = \frac{1}{2}(f_{ij} + f_{ji})$$

- r_{ij} is the microrotation:

$$r_{ij} = \frac{1}{2}(f_{ij} - f_{ji})$$

- h_{ijk} is the (micro) second gradient:

$$h_{ijk} = \frac{\partial f_{ij}}{\partial x_k}$$

- The internal virtual work (Germain, 1973)

$$W^{*\mathrm{i}} = \int_{\Omega} w^* \, \mathrm{d}v = \int_{\Omega} (\sigma_{ij} D^*_{ij} + \tau_{ij}(f^*_{ij} - F^*_{ij}) + \chi_{ijk} h^*_{ijk}) \, \mathrm{d}v$$

- The external virtual work (simplified)

$$W^{*\mathrm{e}} = \int_{\Omega} G_i u^*_i \, \mathrm{d}v + \int_{\partial\Omega} (t_i u^*_i + T_{ij} f^*_{ij}) \, \mathrm{d}s$$

- The virtual work equations can be extended to large strain problems

- Balance equations

$$\begin{cases} \dfrac{\partial(\sigma_{ij} - \tau_{ij})}{\partial x_j} + G_i = 0 \\ \dfrac{\partial \chi_{ijk}}{\partial x_k} - \tau_{ij} = 0 \end{cases}$$

- Boundary conditions

$$\begin{cases} (\sigma_{ij} - \tau_{ij}) n_j = t_i \\ \chi_{ijk} n_k = T_{ij} \end{cases}$$

written in the current configuration

Three constitutive equations needed !

- Local second gradient models: we add the kinematical constraint:

$$f_{ij} = F_{ij}$$

this implies:

$$f_{ij} = \frac{\partial u_i}{\partial x_j}$$

the virtual work equation reads

$$\int_\Omega \left(\sigma_{ij} D^*_{ij} + \chi_{ijk} \frac{\partial^2 u^*_i}{\partial x_j \partial x_k} \right) \mathrm{d}v = \int_\Omega G_i u^*_i \, \mathrm{d}v + \int_{\partial\Omega} (p_i u^*_i + P_i D u^*_i) \, \mathrm{d}s$$

- Local second gradient models

balance equations

$$\frac{\partial \sigma_{ij}}{\partial x_j} - \frac{\partial^2 \chi_{ijk}}{\partial x_j \partial x_k} + G_i = 0$$

boundary conditions

$$\sigma_{ij} n_j - \left(n_k n_j D\chi_{ijk} - \frac{D\chi_{ijk}}{Dx_k} n_j - \frac{D\chi_{ijk}}{Dx_j} n_k + \frac{Dn_l}{Dx_l} \chi_{ijk} n_j n_k - \frac{Dn_j}{Dx_k} \chi_{ijk} \right) = p_i$$

$$\chi_{ijk} n_j n_k = P_i$$

How do we introduce an internal length scale in second grade model ?

Let's take a simple example of a 1D-bar in traction:

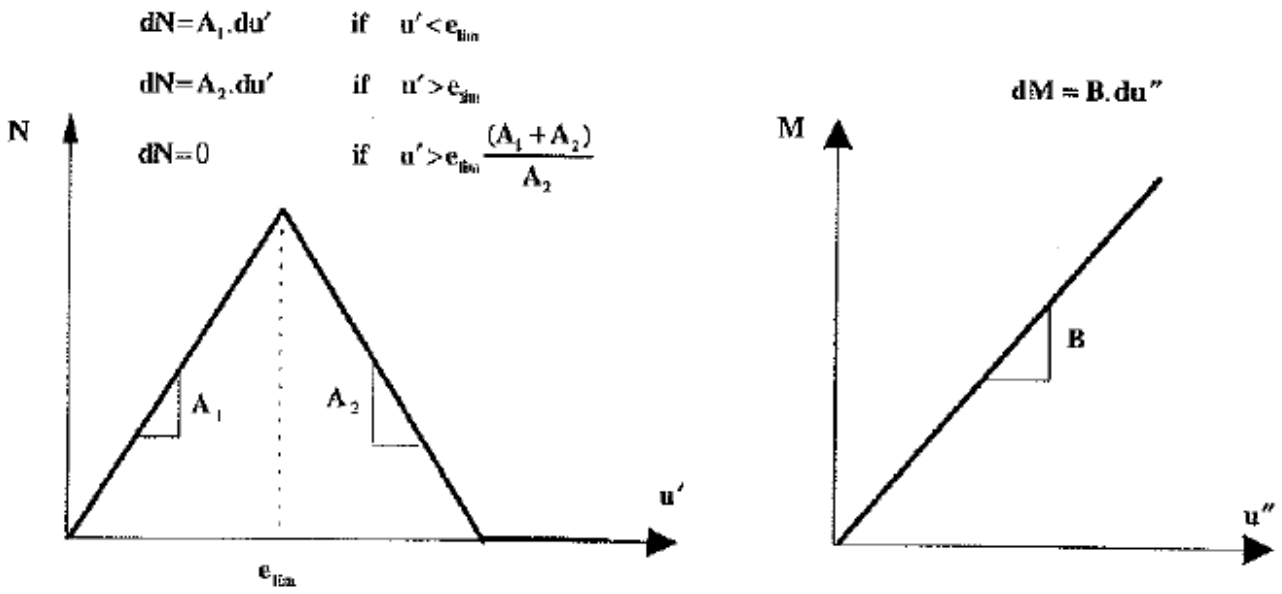

General differential equation of the problem $Au - Bu'' = N_1 x + AK$

Where $N_1 = N - M' = \text{Cst}$, $K = \text{Cst}$, $A = A_1$ if $u' < e_{lim}$ and $A = A_2$ if $u' > e_{lim}$

General solution of the problem

$$u = (N_1/A_1)x + K + \alpha \cosh(\omega x) + \beta \sinh(\omega x); \qquad \omega^2 = A_1/B > 0$$

if $u' < e_{lim}$

$$u = (N_1/A_1)x + K + \alpha \cos(\eta x) + \beta \sin(\eta x); \qquad -\eta^2 = A_2/B < 0$$

if $u' > e_{lim}$

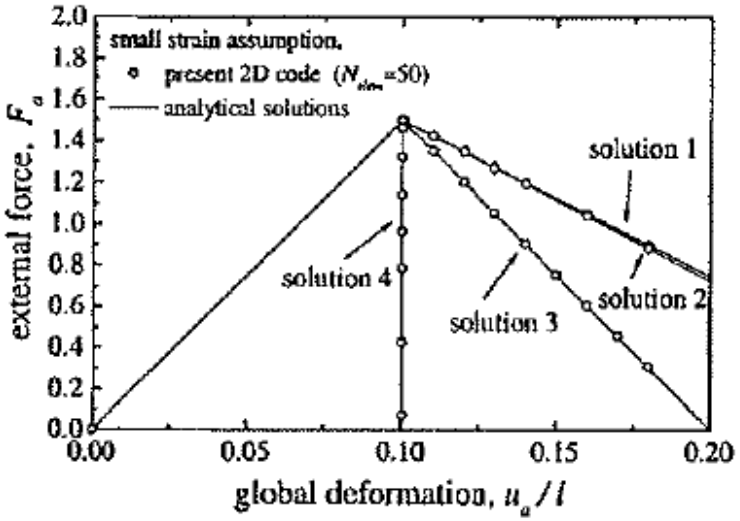

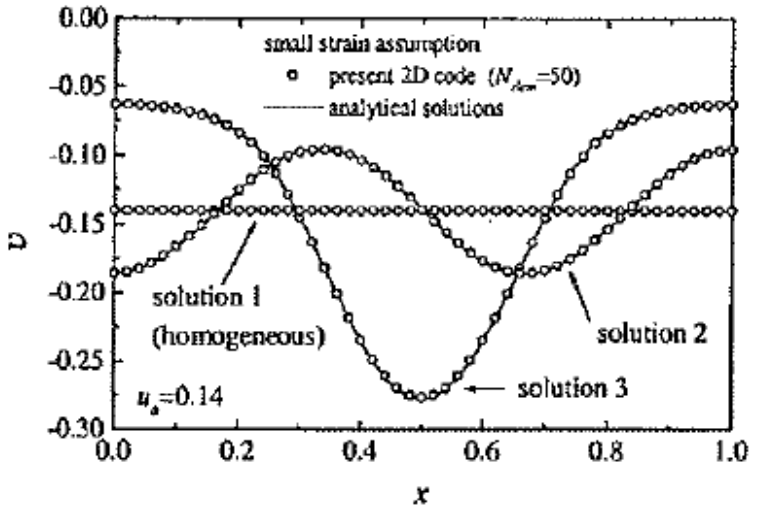

Let's take another example: thick-walled cylinder problem (elastic second gradient model)

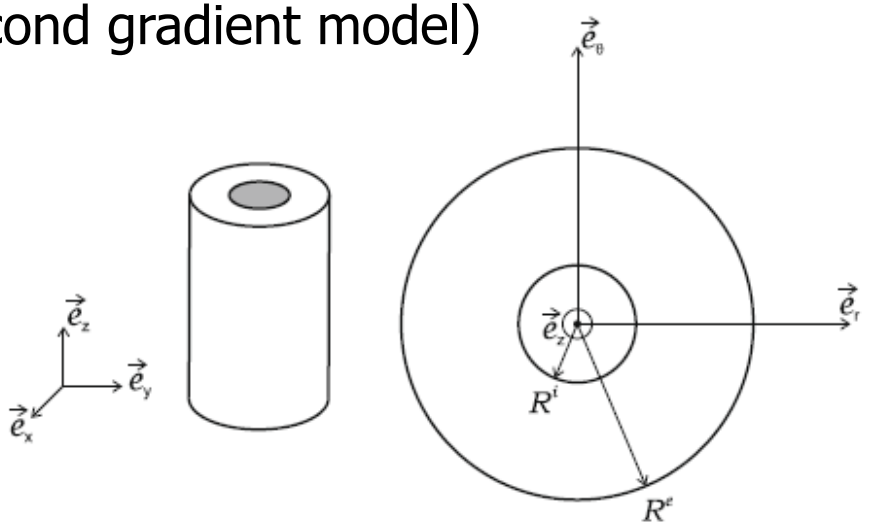

Balance equation $$\partial_r(r\sigma_{rr}) - \sigma_{\theta\theta} + \frac{1}{r}\partial_r(r(\chi_{\theta\theta r} + \chi_{r\theta\theta} + \chi_{\theta r\theta})) - \partial_r^2(r\chi_{rrr}) = 0$$

General differential equation of the problem $$(\lambda + 2\mu)r\partial_r v - Ar\partial_r\left(\frac{1}{r}\partial_r(r\partial_r v)\right) = 0$$

$$v = \frac{1}{r}\partial_r(ru)$$

General solution $$u = C_1 B^I\left(1, \frac{r}{\alpha}\right) + C_2 B^K\left(1, \frac{r}{\alpha}\right) + C_3 r + \frac{C_4}{r} \qquad \alpha = \sqrt{\frac{A}{\lambda + 2\mu}}$$

Finite element formulation of a second grade model

- ***Local second gradient model :*** *additional assumption* $v_{ij}^* = F_{ij}^*$

$$\int_\Omega \left(\sigma_{ij} \frac{\partial u_i^*}{\partial x_j} + \Sigma_{ijk} \frac{\partial^2 u_i^*}{\partial x_j \partial x_k} \right) d\Omega = W_{ext}^*$$

Local quantities

Introduction of Lagrange multiplier field :

$$\int_\Omega \left(\sigma_{ij} \frac{\partial u_i^*}{\partial x_j} + \Sigma_{ijk} \frac{\partial v_{ij}^*}{\partial x_k} \right) d\Omega - \int_\Omega \lambda_{ij} \left(\frac{\partial u_i^*}{\partial x_j} - v_{ij}^* \right) d\Omega = W_{ext}^*$$

$$\int_\Omega \lambda_{ij}^* \left(\frac{\partial u_i}{\partial x_j} - v_{ij} \right) d\Omega = 0$$

Local Second gradient Finite element

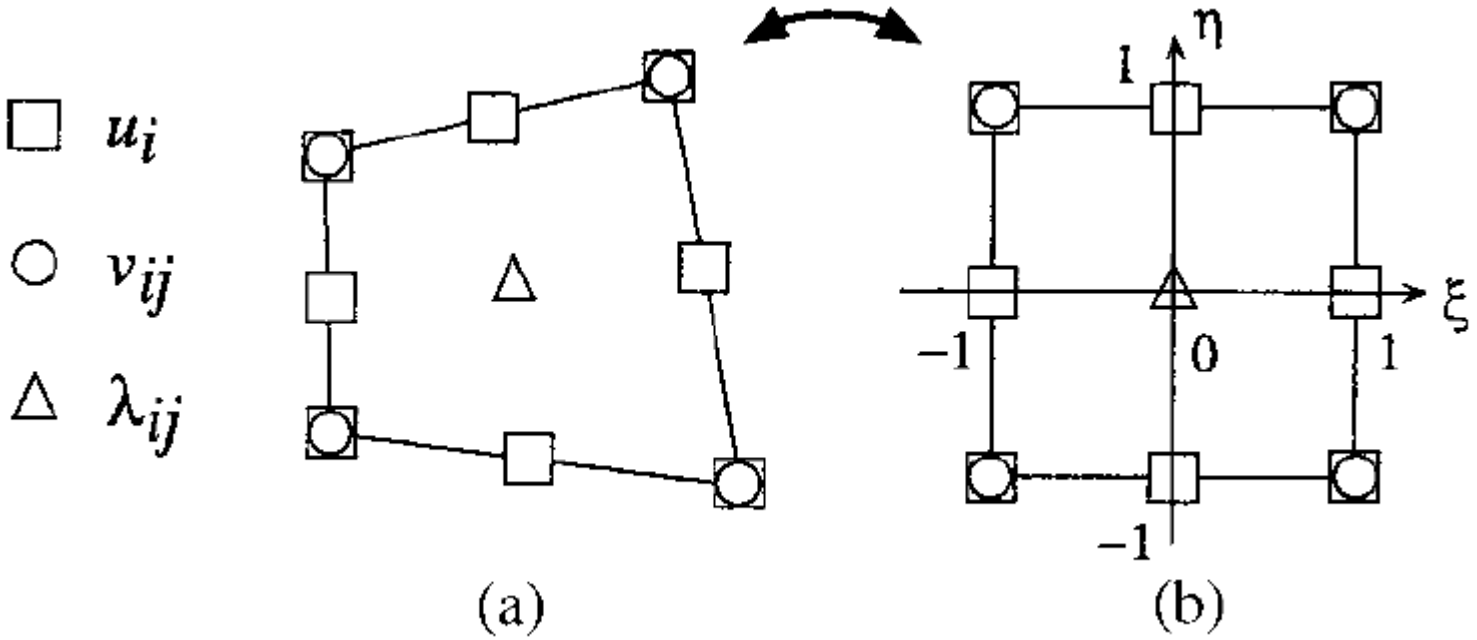

- *Biaxial compression test*

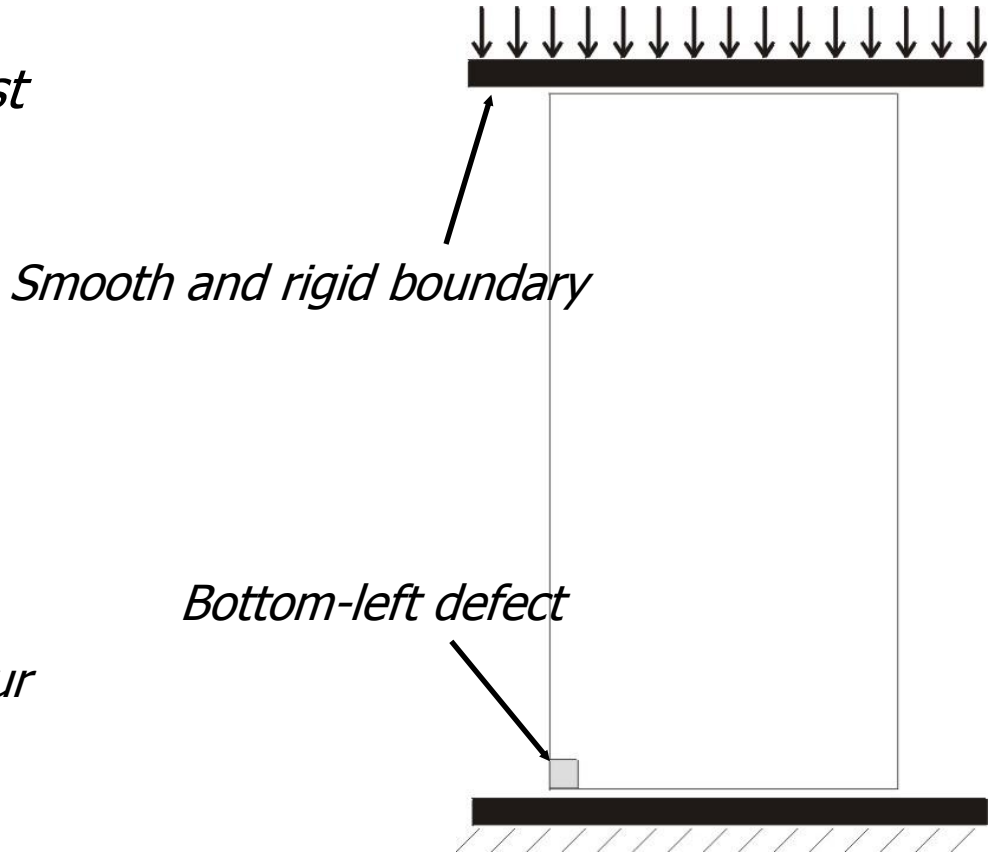

Strain rate : 0.18% / hour

No lateral confinement

Globally drained (upper and lower drainage)

- *First gradient law :*

Linear elasticity : E_0 *and* ν_0

Drucker Prager criterion :

$$F \equiv \sqrt{\frac{3}{2}} II_{\hat{\sigma}} + m\left(I_\sigma - \frac{3c}{\tan\phi} \right) = 0$$

$$m = \frac{2\sin\phi}{3-\sin\phi} \qquad c = c_0 f(\gamma^p)$$

Associated softening plasticity (decrease of cohesion) :

$$f(\gamma^p) = \left(1-(1-\alpha)\frac{\gamma^p}{\gamma_R^p} \right)^2 si\ 0 < \gamma^p < \gamma_R^p$$

$$= \alpha^2\ si\ \gamma^p \geq \gamma_R^p$$

E = 5800 MPa
ν = 0,3

ϕ = 25°
Ψ = 25°

c_0 = 1 MPa
α = 0,01
γ_R = 0,015

- *Second gradient law :* *Linear relationship deduced from Mindlin*

$$\begin{bmatrix} \tilde{\Sigma}_{111} \\ \tilde{\Sigma}_{112} \\ \tilde{\Sigma}_{121} \\ \tilde{\Sigma}_{122} \\ \tilde{\Sigma}_{211} \\ \tilde{\Sigma}_{212} \\ \tilde{\Sigma}_{221} \\ \tilde{\Sigma}_{222} \end{bmatrix} = \begin{bmatrix} D & 0 & 0 & 0 & 0 & \frac{D}{2} & \frac{D}{2} & 0 \\ 0 & \frac{D}{2} & \frac{D}{2} & 0 & -\frac{D}{2} & 0 & 0 & \frac{D}{2} \\ 0 & \frac{D}{2} & \frac{D}{2} & 0 & -\frac{D}{2} & 0 & 0 & \frac{D}{2} \\ 0 & 0 & 0 & D & 0 & -\frac{D}{2} & -\frac{D}{2} & 0 \\ 0 & -\frac{D}{2} & -\frac{D}{2} & 0 & D & 0 & 0 & 0 \\ \frac{D}{2} & 0 & 0 & -\frac{D}{2} & 0 & \frac{D}{2} & \frac{D}{2} & 0 \\ \frac{D}{2} & 0 & 0 & -\frac{D}{2} & 0 & \frac{D}{2} & \frac{D}{2} & 0 \\ 0 & \frac{D}{2} & \frac{D}{2} & 0 & 0 & 0 & 0 & 0 \end{bmatrix} \begin{bmatrix} \frac{\partial \dot{v}_{11}}{\partial x_1} \\ \frac{\partial \dot{v}_{11}}{\partial x_2} \\ \frac{\partial \dot{v}_{12}}{\partial x_1} \\ \frac{\partial \dot{v}_{12}}{\partial x_2} \\ \frac{\partial \dot{v}_{21}}{\partial x_1} \\ \frac{\partial \dot{v}_{21}}{\partial x_2} \\ \frac{\partial \dot{v}_{22}}{\partial x_1} \\ \frac{\partial \dot{v}_{22}}{\partial x_2} \end{bmatrix}$$

D = 20 kN

First modelling: no HM coupling (no overpressure)

Bifurcation directions

(Regularization : Second gradient)

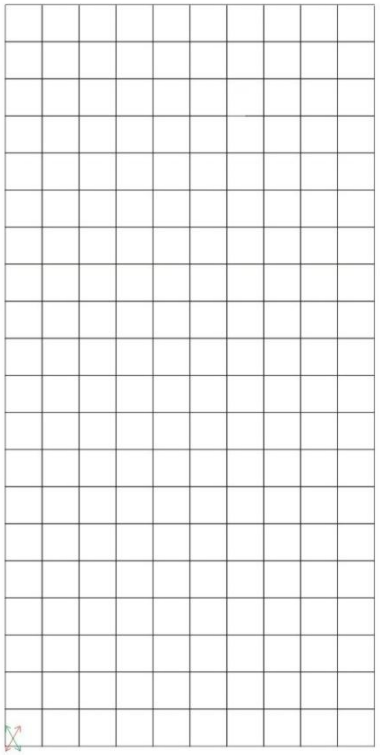

Before

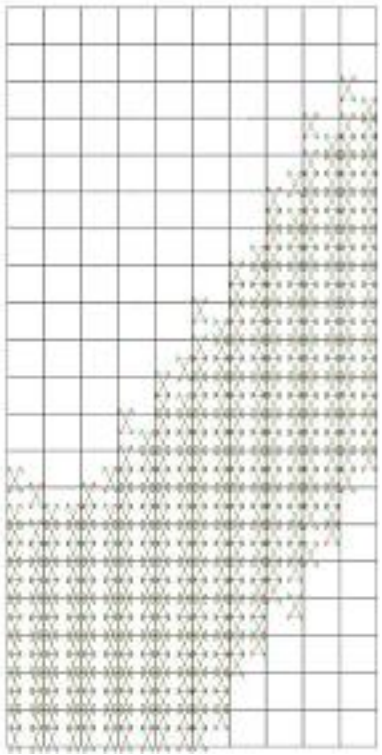

After

First modelling: no HM coupling (no overpressure)

Plastic loading point

(Regularization : Second gradient)

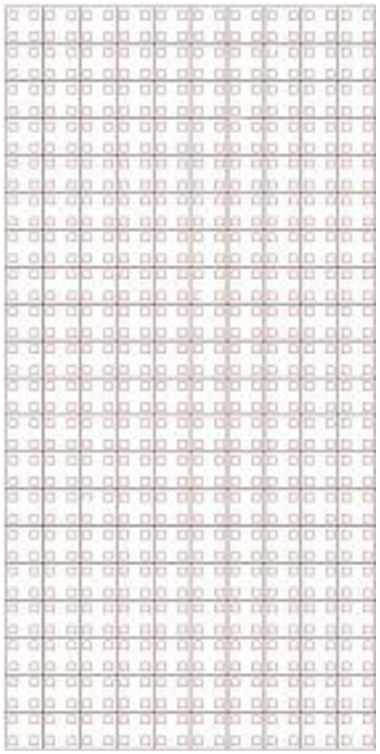

Before

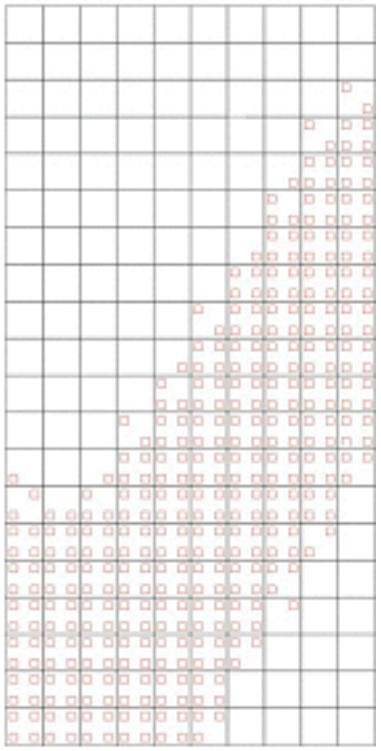

After

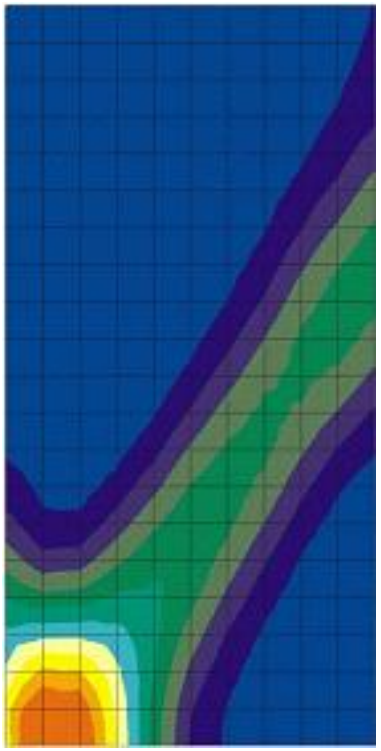

First modelling: no HM coupling (no overpressure)

Velocitiy field

(Regularization : Second gradient)

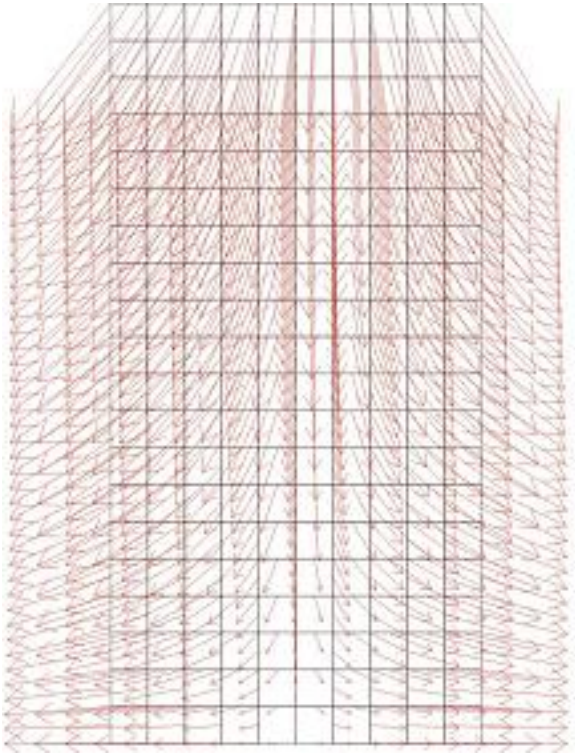

Before

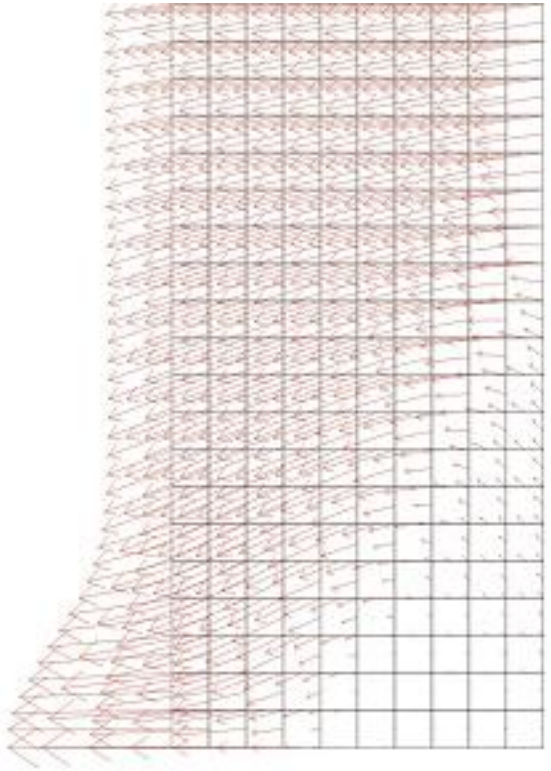

After

Initiation of localization (Directional research)

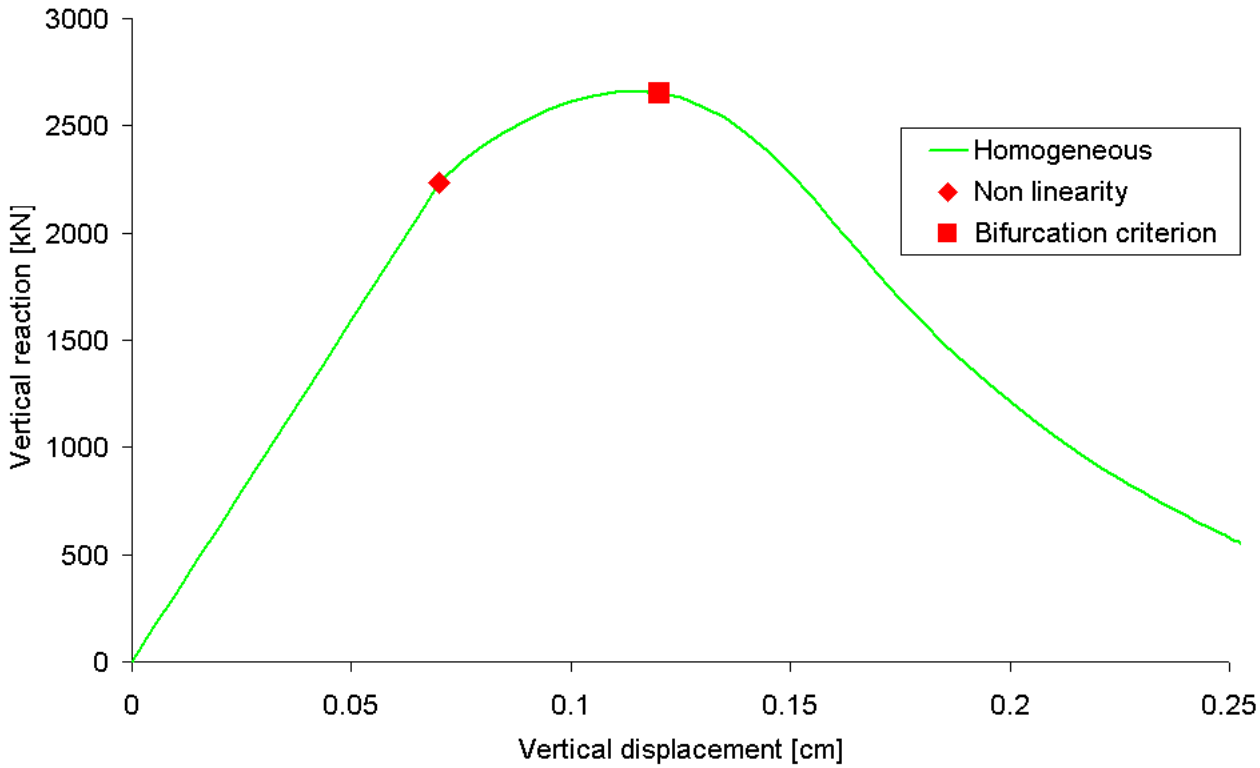

Initiation of localization (Directional research)

(Regularization : Second gradient)

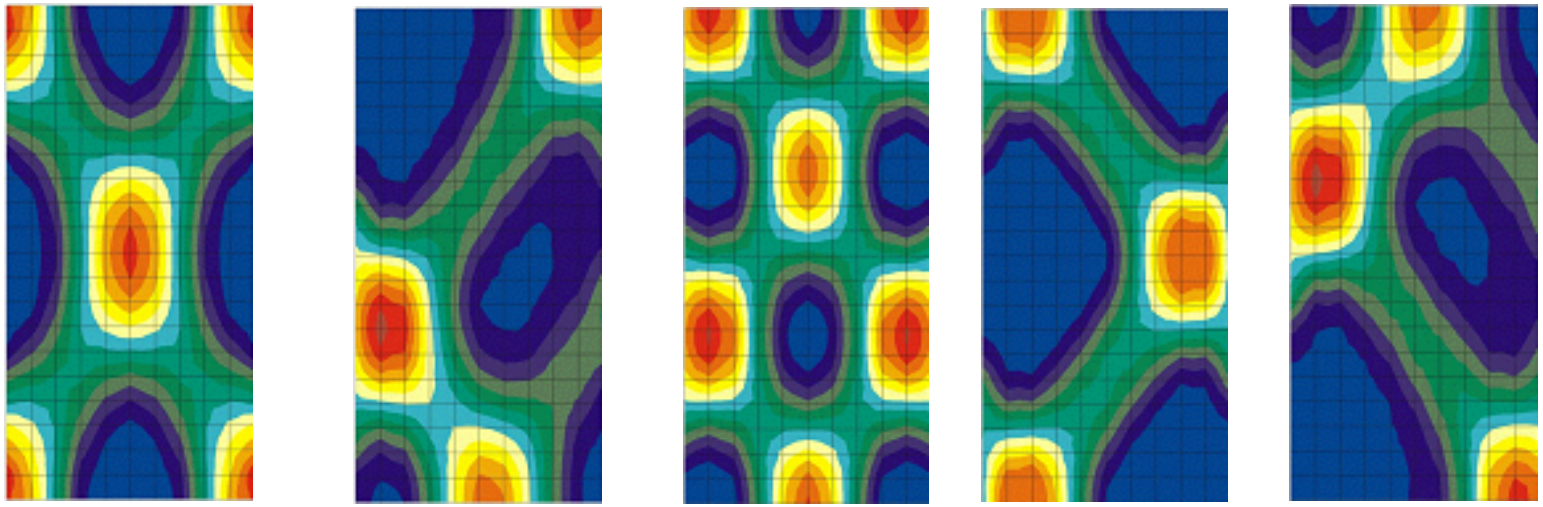

Non uniqueness of the solution

Initiation of localization (Directional research)

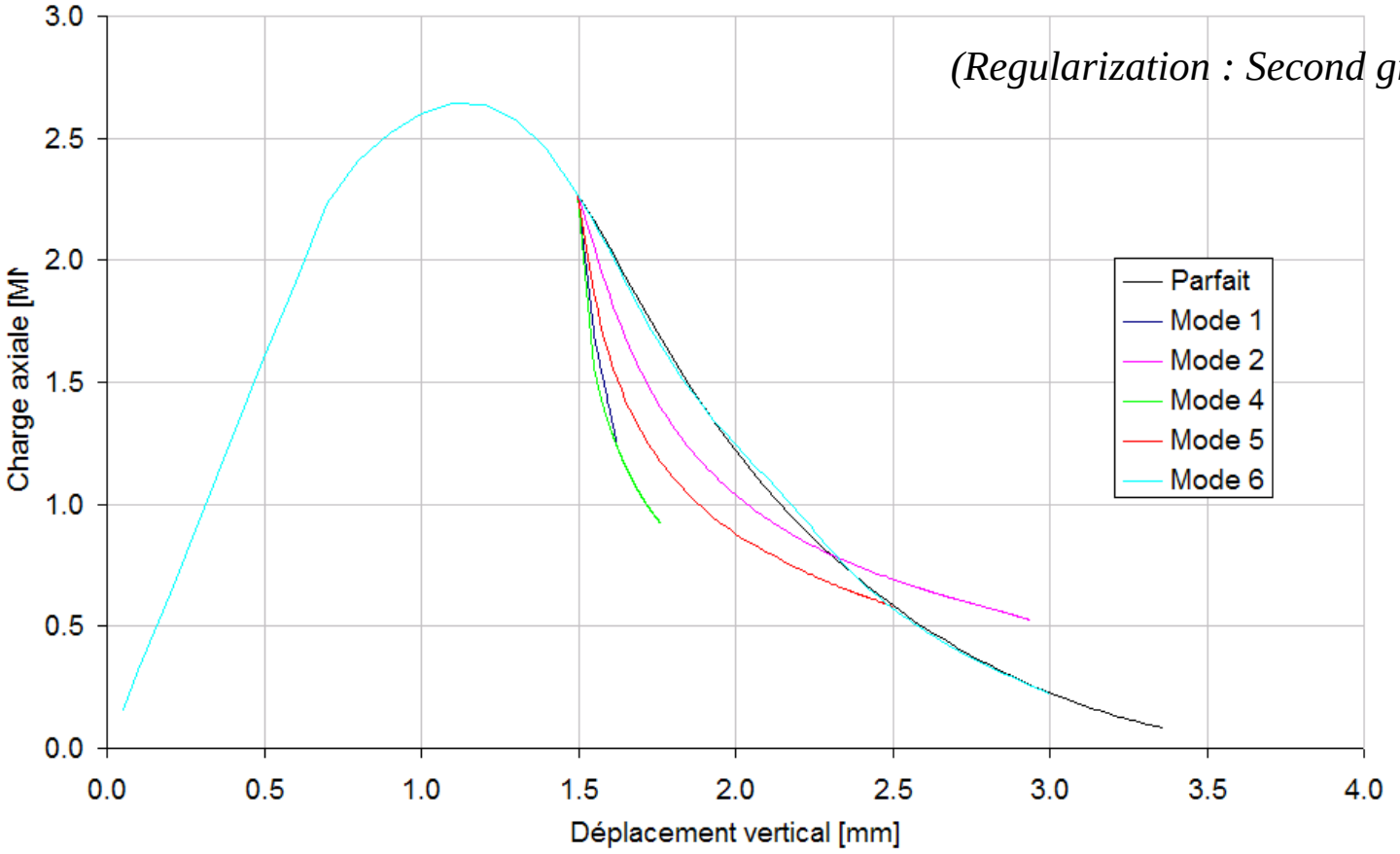

Non uniqueness of the solution

Initiation of localization (Directional research)

(Regularization : Second gradient)

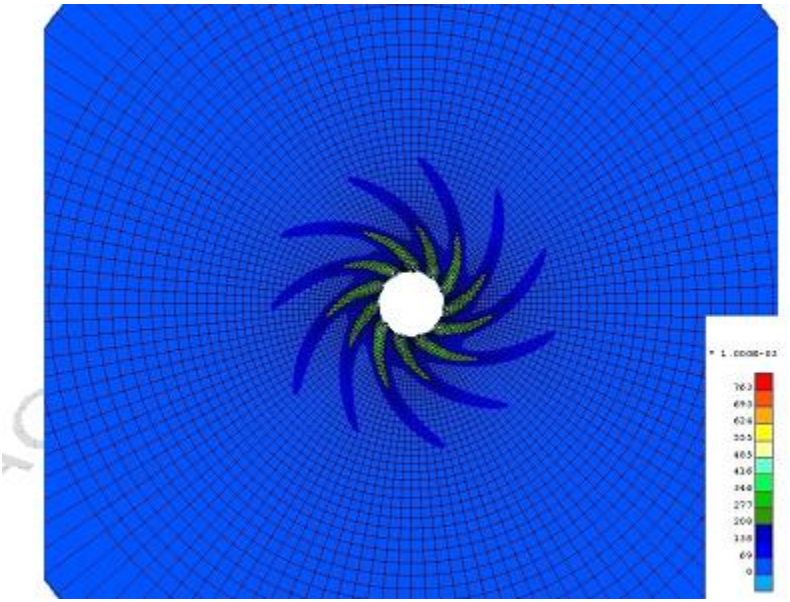

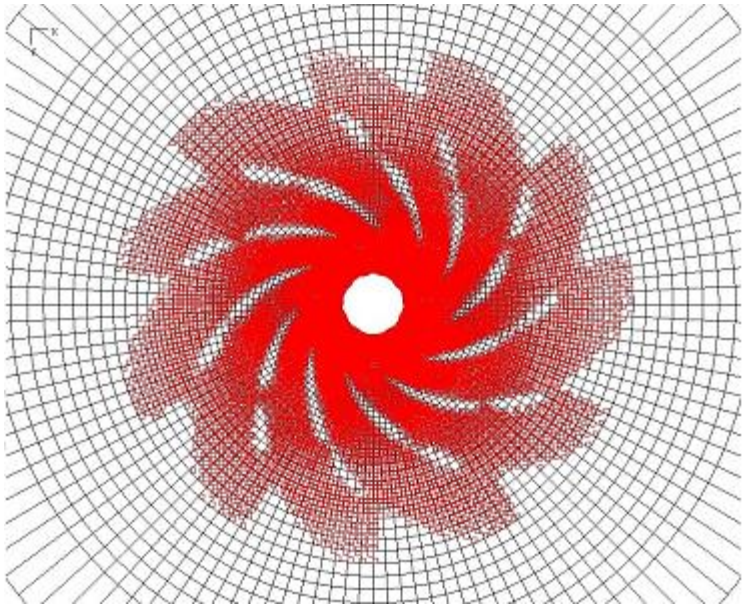

Non uniqueness of the solution

Sieffert et al., 2009

Our goal is to extend the second gradient formulation for multiphysics conditions. In the following, we focus on the hydromechanical model but the same procedure can be applied for TM, THM or THMC problems.

- ***Main assumptions***
  - *Quasi static motion*
  - *Fully saturated*
  - *Incompressible solid grains*
- ***Aims***
  - *Equations written in the spatial configuration*
  - *Full Newton Raphson method*

- ***Classical poromechanics field equations***

Saturated porous medium

Balance of linear momentum for the mixture

$$\int_{\Omega} \sigma_{ij} \varepsilon_{ij}^{*} d\Omega = \int_{\Omega} \rho_{mix} g_i u_i^{*} d\Omega + \int_{\Gamma} \bar{t}_i u_i^{*} d\Gamma$$

Boundary condition $\sigma_{ij} n_j = \bar{t}_i$

Terzaghi's postulate $\sigma_{ij} = \sigma'_{ij} - p\delta_{ij}$

- ***Classical poromechanics field equations***

Fluid mass balance

$$\int_\Omega \dot{M}\ p^* - m_i \frac{\partial p^*}{\partial x_i} d\Omega = \int_\Omega Q\, p^* d\Omega + \int_\Gamma \bar{q}\ p^* d\Gamma$$

Boundary condition $\bar{q} = m_i n_i$

Darcy's law $m_i = -\rho_w \frac{\kappa}{\mu}\left(\frac{\partial p}{\partial x_i} + \rho_w g_i\right)$

Storage law $\dot{M} = \rho_w \frac{\dot{p}}{k^w}\phi + \rho_w \frac{\dot{\Omega}}{\Omega}$

- ***Classical poromechanics field equations***

Balance of momentum for the fluid phase

$$\frac{\partial p^t}{\partial x_i^t} + F_i^{S/W,t} + \varrho^{w,t} g_i = 0$$

Viscous drag force : $$F_i^{S/W,t} = \frac{\varrho^{w,t} \phi^t g}{K} V_i^{W/S,t}$$

Mass balance equation for the solid

$$\frac{\partial(\rho_s(1-\phi^t)\Omega^t)}{\partial t} = 0$$

- ***Coupled local second gradient model***

  - ✓ Second gradient effects are assumed only for solid phase
  - ✓ For the mixture, there are stresses which obey the Terzaghi postulate and double stresses which are only the one of the solid phase
  - ✓ Boundary conditions for the mixture are enriched

- *Coupled local second gradient model*

$$\int_\Omega \left(\sigma_{ij} \frac{\partial u_i^*}{\partial x_j} + \Sigma_{ijk} \frac{\partial^2 u_i^*}{\partial x_j \partial x_k} \right) d\Omega = \int_\Omega \rho_{mix} g_i u_i^* d\Omega + \int_\Gamma \bar{t}_i u_i^* + \bar{T}_i D u_i^* d\Gamma$$

$$\int_\Omega \dot{M}\ p^* - m_i \frac{\partial p^*}{\partial x_i} d\Omega = \int_\Omega Q\, p^* d\Omega + \int_\Gamma \bar{q}\ p^* d\Gamma$$

- *Coupled local second gradient model*

$$\int_\Omega \left(\sigma_{ij} \frac{\partial u_i^*}{\partial x_j} + \Sigma_{ijk} \frac{\partial v_{ij}^*}{\partial x_k} \right) d\Omega - \int_\Omega \lambda_{ij} \left(\frac{\partial u_i^*}{\partial x_j} - v_{ij}^* \right) d\Omega =$$

$$\int_\Omega \rho_{mix} g_i u_i^* d\Omega + \int_\Gamma \bar{t}_i u_i^* + \bar{T}_i D u_i^* d\Gamma$$

$$\int_\Omega \dot{M}\ p^* - m_i \frac{\partial p^*}{\partial x_i} d\Omega = \int_\Omega Q\, p^* d\Omega + \int_\Gamma \bar{q}\ p^* d\Gamma$$

$$\int_\Omega \lambda_{ij}^* \left(\frac{\partial u_i}{\partial x_j} - v_{ij} \right) d\Omega = 0$$

Finite element formulation of the coupled local second gradient model

- ✓ *Equations are assumed to be met at time t*
- ✓ *We are looking for the values of the different fields at time: $t+\Delta t=\tau_1$*
- ✓ *using a full Newton Raphson method and an implicit scheme for the rate :*

$$\dot{p}^{t+\Delta t} = \frac{p^{t+\Delta t} - p^t}{\Delta t}$$

- *Field equations at time t+Δt*

$$\int_{\Omega^{\tau 1}} \left(\sigma_{ij}^{\tau 1} \frac{\partial u_i^*}{\partial x_j^{\tau 1}} + \Sigma_{ijk}^{\tau 1} \frac{\partial v_{ij}^*}{\partial x_k^{\tau 1}} \right) d\Omega^{\tau 1} - \int_{\Omega^{\tau 1}} \lambda_{ij}^{\tau 1} \left(\frac{\partial u_i^*}{\partial x_j^{\tau 1}} - v_{ij}^* \right) d\Omega^{\tau 1} -$$

$$\int_{\Omega^{\tau 1}} (\varrho^s (1-\phi^{\tau 1}) + \varrho^{w,\tau 1} \phi^{\tau 1}) g_i u_i^* d\Omega^{\tau 1} - \int_{\Gamma^{\tau 1}} \left(\overline{t}_i u_i^* + \overline{T}_i v_{ik}^* n_k^{\tau 1} \right) d\Gamma^{\tau 1} = R^{\tau 1},$$

$$\int_{\Omega^{\tau 1}} \lambda_{ij}^* \left(\frac{\partial u_i}{\partial x_j^{\tau 1}} - v_{ij}^{\tau 1} \right) d\Omega^{\tau 1} = S^{\tau 1},$$

$$\int_{\Omega^{\tau 1}} (\dot{M}^{\tau 1} p^\star - m_i^{\tau 1} \frac{\partial p^\star}{\partial x_i^{\tau 1}}) d\Omega^{\tau 1} - \int_{\Omega^{\tau 1}} Q^{\tau 1} p^\star d\Omega^{\tau 1} + \int_{\Gamma_q^{\tau 1}} \overline{q}^{\tau 1} p^\star d\Gamma^{\tau 1} = W^{\tau 1}.$$

R, S and W : Residuals of the balance equations

- *Linearization of field equations*

→ *Auxiliary linear problem*

$$\int_{\Omega} \left[U^{*}_{(x,y)} \right]^{T} [E] \left[dU_{(x,y)} \right] d\Omega = -R - S - W$$

R, S and W : Residuals of the balance equations

$$\left[dU_{(x,y)} \right] = \left[\frac{\partial du_1}{\partial x_1} \frac{\partial du_1}{\partial x_2} \frac{\partial du_2}{\partial x_1} \frac{\partial du_2}{\partial x_2} du_1 \, du_2 \frac{\partial dp}{\partial x_1} \frac{\partial dp}{\partial x_2} dp \right.$$

$$\left. \frac{\partial dv_{11}}{\partial x_1} \frac{\partial dv_{11}}{\partial x_2} \frac{\partial dv_{12}}{\partial x_1} \cdots \frac{\partial dv_{22}}{\partial x_2} dv_{11} \cdots dv_{22} \; d\lambda_{11} \cdots d\lambda_{22} \right]$$

$$[E] = \begin{bmatrix} E1_{(4x4)} & 0_{(4x2)} & K_{WM\,(4x3)} & 0_{(4x8)} & 0_{(4x4)} & -I_{(4x4)} \\ G1_{(2x4)} & 0_{(2x2)} & G2_{(2x3)} & 0_{(2x8)} & 0_{(2x4)} & 0_{(2x4)} \\ K_{MW\,(3x4)} & 0_{(3x2)} & K_{WW\,(3x3)} & 0_{(3x8)} & 0_{(3x4)} & 0_{(3x4)} \\ E2_{(8x4)} & 0_{(8x2)} & 0_{(8x3)} & D_{(8x8)} & 0_{(8x4)} & 0_{(8x4)} \\ E3_{(4x4)} & 0_{(4x2)} & 0_{(4x3)} & 0_{(4x8)} & 0_{(4x4)} & I_{(4x4)} \\ E4_{(4x4)} & 0_{(4x2)} & 0_{(4x3)} & 0_{(4x8)} & -I_{(4x4)} & 0_{(4x4)} \end{bmatrix}$$

E1, E2, E3, E4 and D : see monophasic local sec. Gradient model

G1 and G2 : related to gravity volume force

K_{WW} : Classical flow matrix

K_{MW} and K_{WM} : Coupling terms including large strain effect

Isoparametric Finite Element :

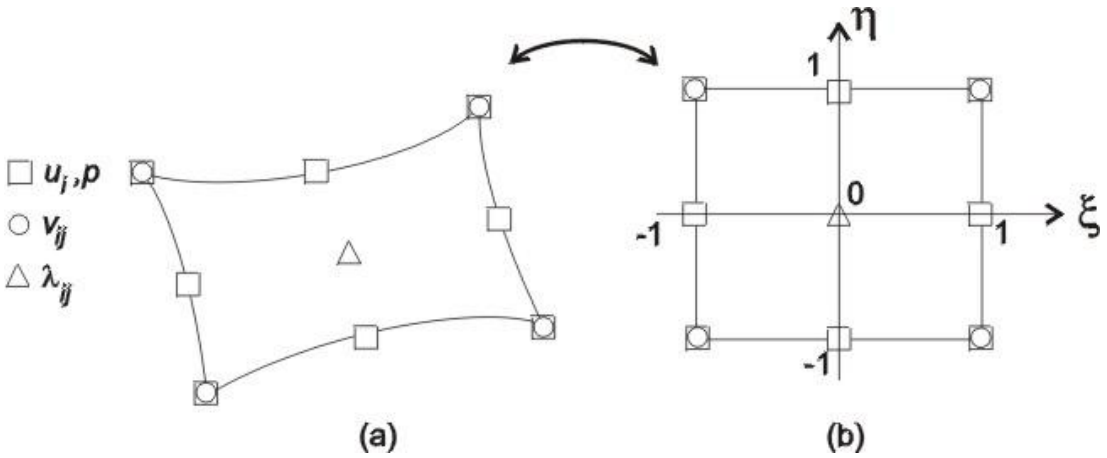

8 nodes for macro-displacement and pressure field
4 nodes for microkinetic gradient field
1 node for Lagrange multipliers field

- *FE element discretization of linear auxiliary problem*

$$\left[U^*_{node}\right]^T \int_{-1}^{1}\int_{-1}^{1} [B]^T [T]^T [E][T][B] \det J \; d\xi d\eta \left[dU_{node}\right] \equiv$$

$$\left[U^*_{node}\right]^T [k]\left[dU_{node}\right]$$

Local stiffness matrix

$$-R - S - W = P^*_{ext} - \left[U^*_{node}\right]^T \int_{-1}^{1}\int_{-1}^{1} [B]^T [T]^T [\sigma] \det J \; d\xi d\eta \equiv$$

$$\left[U^*_{node}\right]^T \left[f_{HE}\right]$$

Elementary out of balance forces

- *Biaxial compression test*

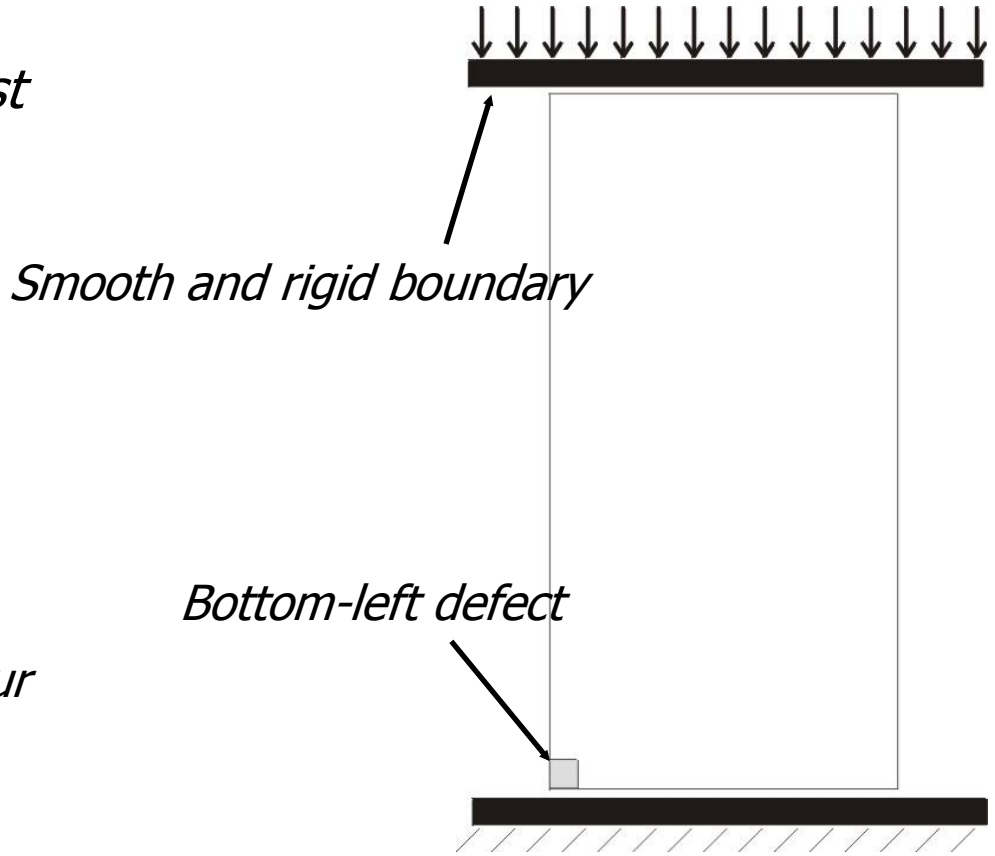

Strain rate : 0.18% / hour

No lateral confinement

Globally drained (upper and lower drainage)

- *Second gradient law :* *Linear relationship deduced from Mindlin*

$$\begin{bmatrix} \tilde{\Sigma}_{111} \\ \tilde{\Sigma}_{112} \\ \tilde{\Sigma}_{121} \\ \tilde{\Sigma}_{122} \\ \tilde{\Sigma}_{211} \\ \tilde{\Sigma}_{212} \\ \tilde{\Sigma}_{221} \\ \tilde{\Sigma}_{222} \end{bmatrix} = \begin{bmatrix} D & 0 & 0 & 0 & 0 & \frac{D}{2} & \frac{D}{2} & 0 \\ 0 & \frac{D}{2} & \frac{D}{2} & 0 & -\frac{D}{2} & 0 & 0 & \frac{D}{2} \\ 0 & \frac{D}{2} & \frac{D}{2} & 0 & -\frac{D}{2} & 0 & 0 & \frac{D}{2} \\ 0 & 0 & 0 & D & 0 & -\frac{D}{2} & -\frac{D}{2} & 0 \\ 0 & -\frac{D}{2} & -\frac{D}{2} & 0 & D & 0 & 0 & 0 \\ \frac{D}{2} & 0 & 0 & -\frac{D}{2} & 0 & \frac{D}{2} & \frac{D}{2} & 0 \\ \frac{D}{2} & 0 & 0 & -\frac{D}{2} & 0 & \frac{D}{2} & \frac{D}{2} & 0 \\ 0 & \frac{D}{2} & \frac{D}{2} & 0 & 0 & 0 & 0 & 0 \end{bmatrix} \begin{bmatrix} \frac{\partial \dot{v}_{11}}{\partial x_1} \\ \frac{\partial \dot{v}_{11}}{\partial x_2} \\ \frac{\partial \dot{v}_{12}}{\partial x_1} \\ \frac{\partial \dot{v}_{12}}{\partial x_2} \\ \frac{\partial \dot{v}_{21}}{\partial x_1} \\ \frac{\partial \dot{v}_{21}}{\partial x_2} \\ \frac{\partial \dot{v}_{22}}{\partial x_1} \\ \frac{\partial \dot{v}_{22}}{\partial x_2} \end{bmatrix}$$

D = 20 kN

- *Flow model parameters*

$\kappa = 10^{-19} / 10^{-12}$ m^2
$\rho_w = 1000$ kg/m^3
$\phi = 0.15$

$k_w = 510^{-10}$ Pa^{-1}
$\mu_w = 0.001$ $Pa.s$

Second modelling: HM coupling

- *Equivalent strain after 0.2 % of axial strain ($\kappa = 10^{-12}$ m²)*

(20 x 10) *(30 x 15)* *(40 x 20)*

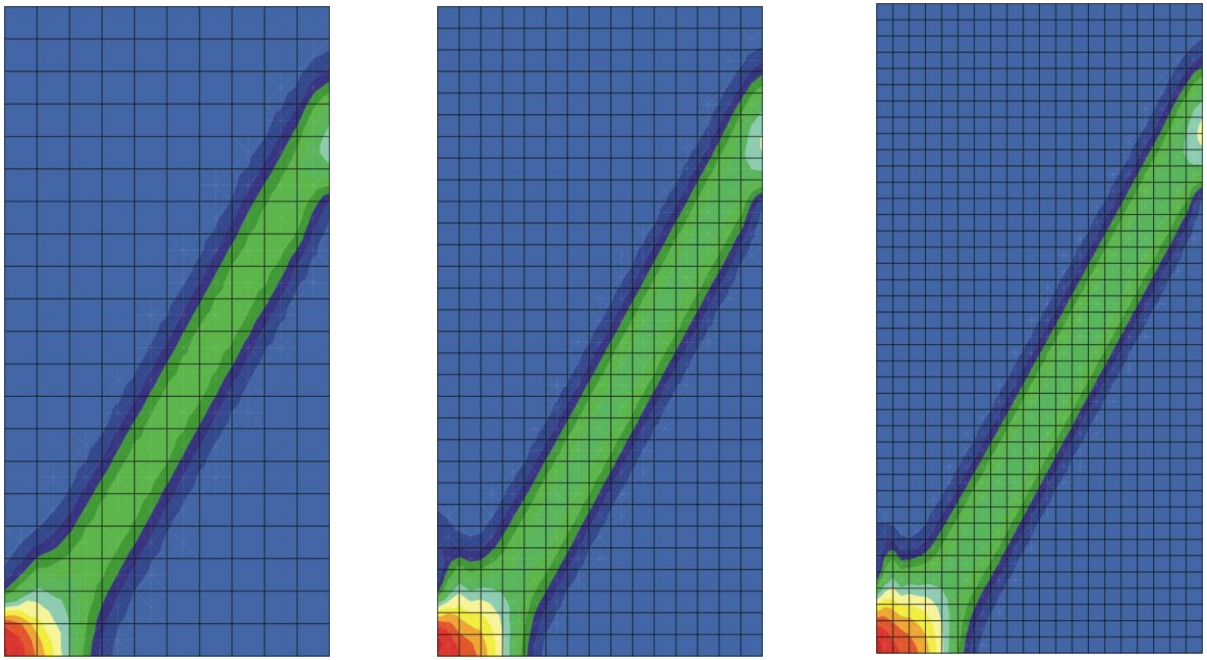

- *Plastic loading point after 0.2 % of axial strain ($\kappa = 10^{-12}$ m²)*

(20 x 10) *(30 x 15)* *(40 x 20)*

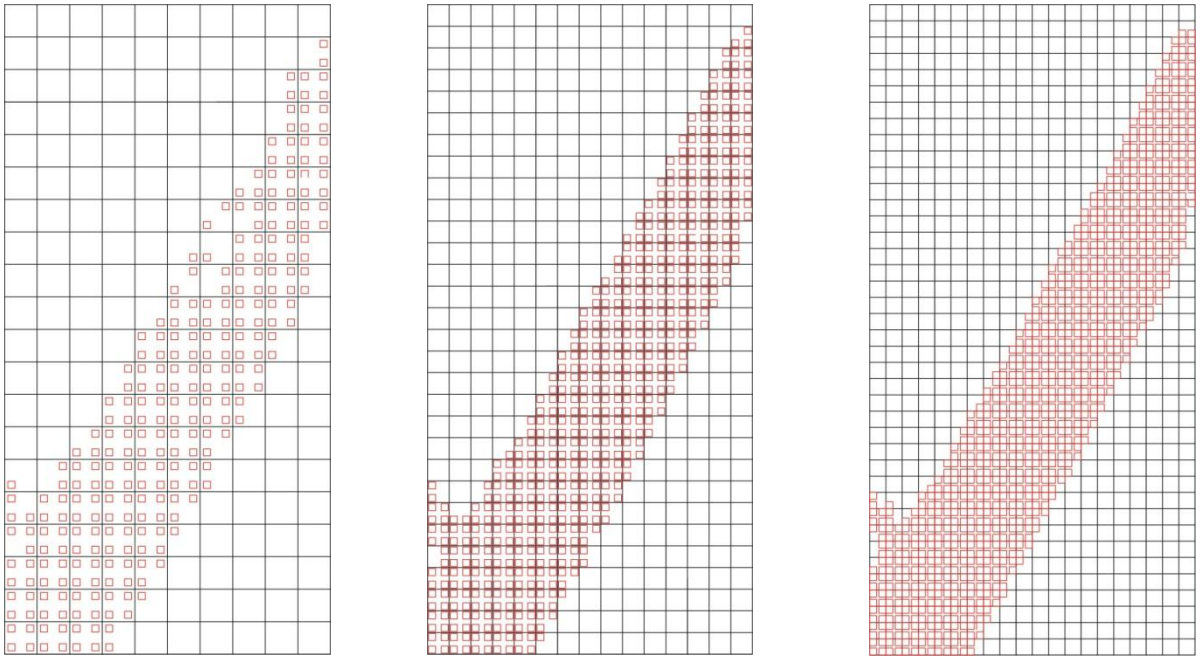

- *Fluid flow after 0.2 % of axial strain ($\kappa = 10^{-12}$ m²)*

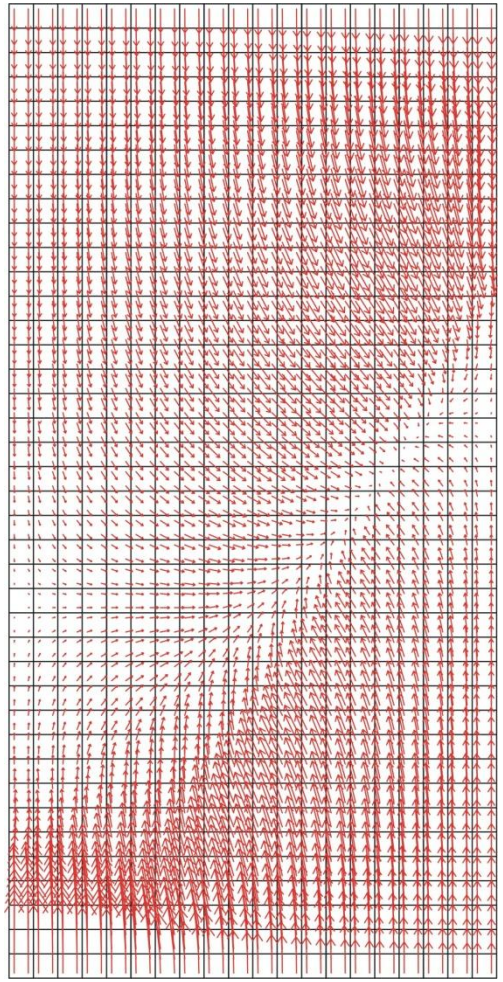

- *Load-displacement curve ($\kappa = 10^{-12}$ m²)*

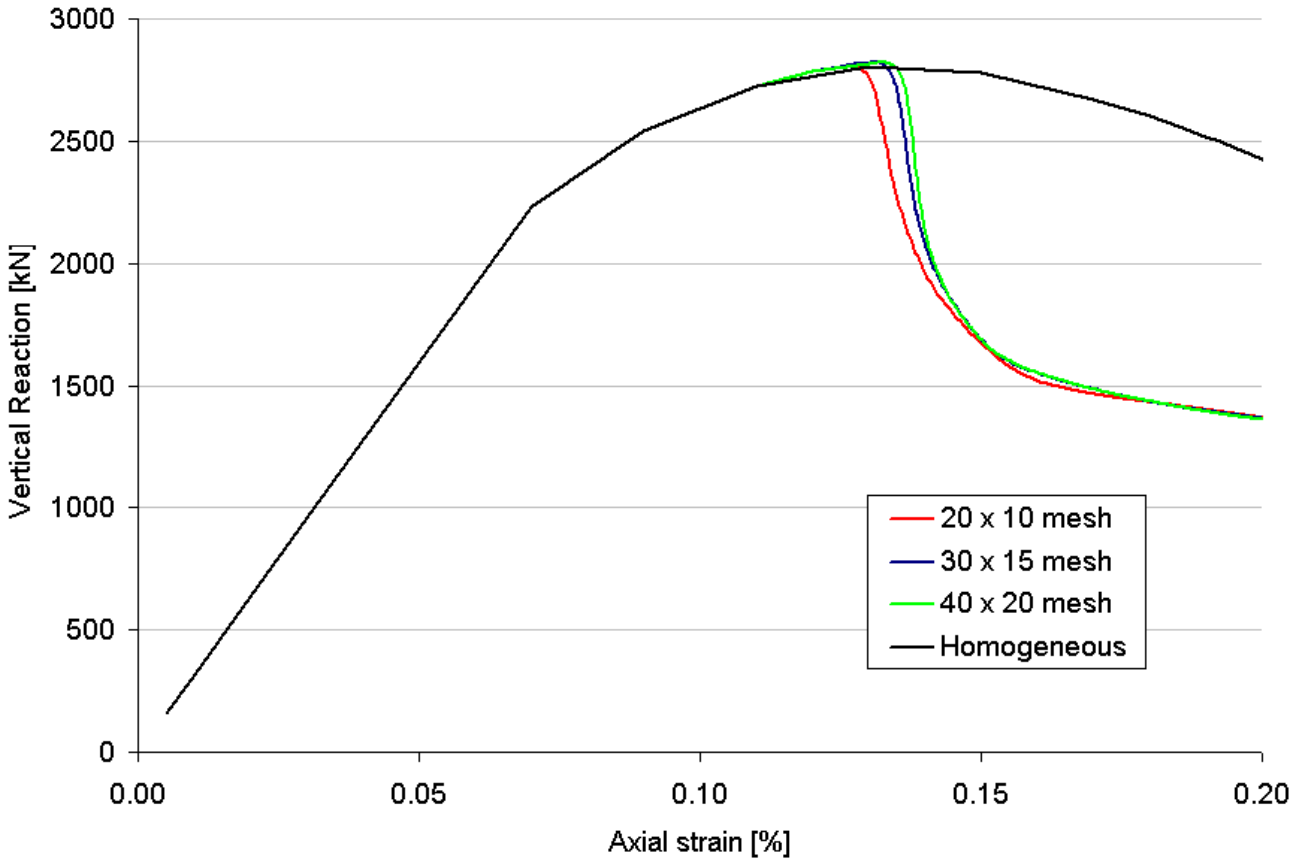

Second modelling: HM coupling

- *Load-displacement curve ($\kappa = 10^{-19}$ m²)*

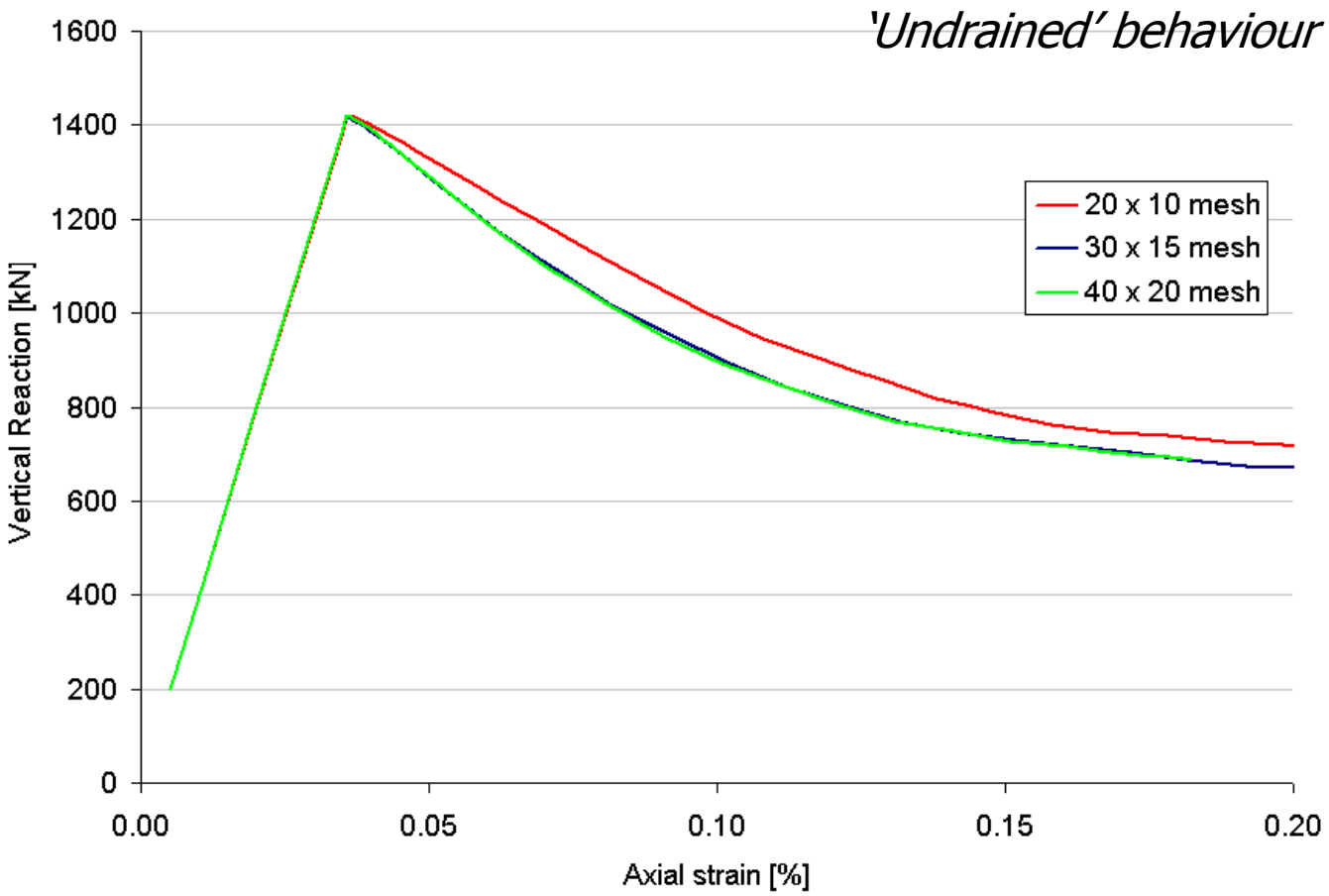

For $\kappa = 10^{-19}\ m^2$, the behaviour is undrained, we recover the experimental observation showing that for dilatant material, no localization is possible before cavitation.

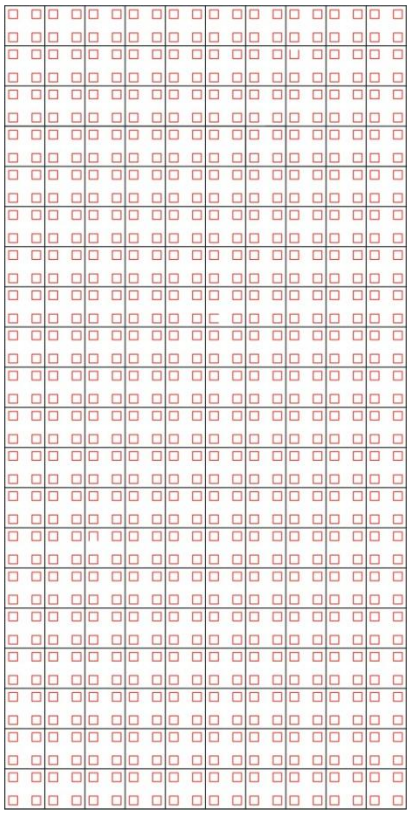

Example of EDZ around a cavity

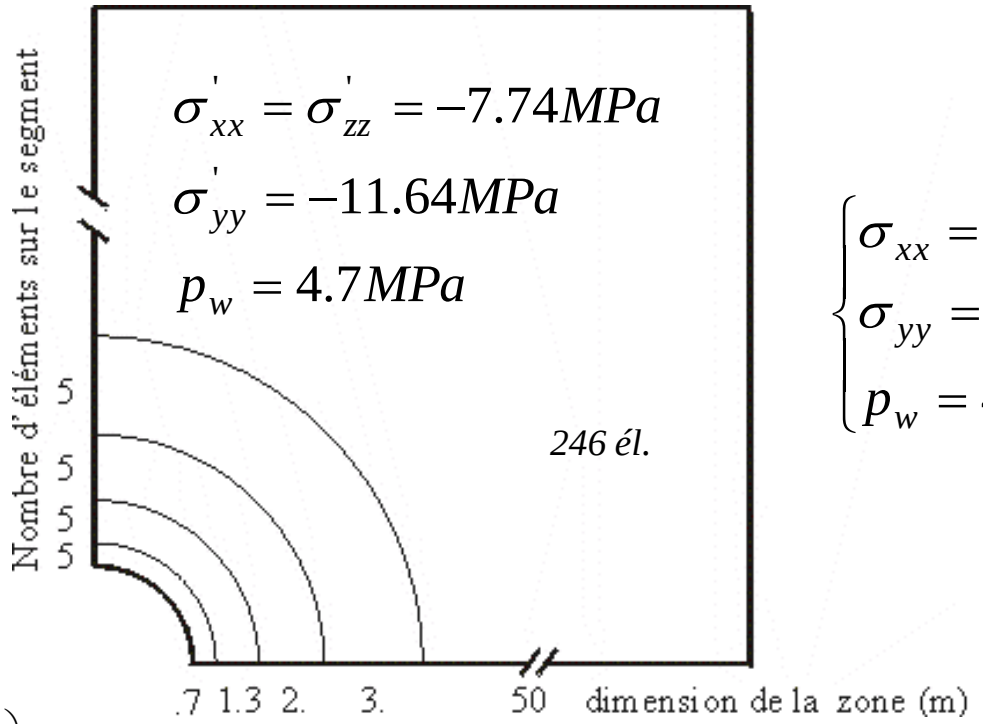

$$\begin{cases} \sigma_{xx} = -11.5MPa \\ \sigma_{yy} = -15.4MPa \\ p_w = 4.7MPa \end{cases}$$

$$\begin{cases} 0 \le t \le T \\ \sigma_{xx} = \sigma'_{xx} - bS_{rw}p_w = -11.5\left(1-\frac{t}{T}\right)MPa \\ \sigma_{yy} = \sigma'_{yy} - bS_{rw}p_w = -15.4\left(1-\frac{t}{T}\right)MPa \\ p_w = 4.7\left(1-\frac{t}{T}\right)MPa \\ t > T \\ \sigma_{xx} = \sigma_{yy} = p_w = 0 \end{cases}$$

T = 1.5 Ms (17 jours)

t_{total} = 300 Ms (9.5 ans)

Coupled modelling – Comparison Coarse mesh - Refined mesh

Classical FE formulation

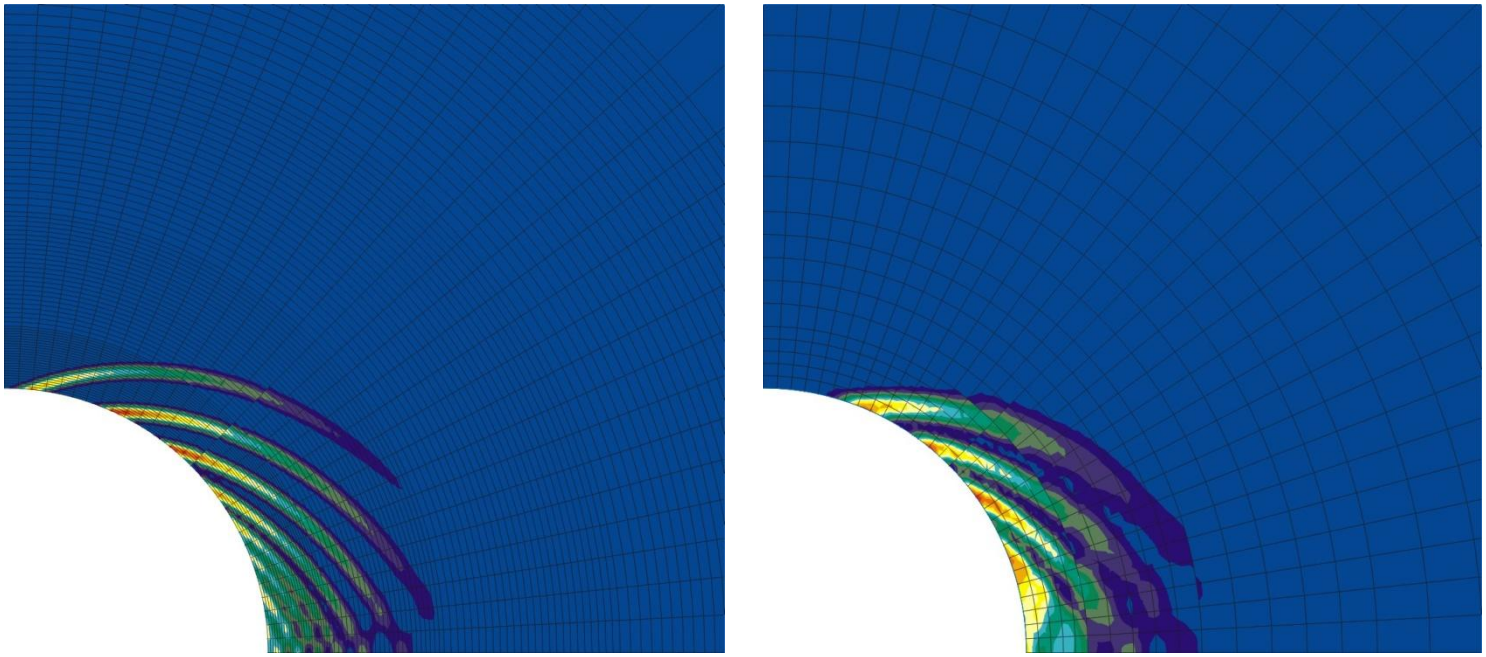

Deviatoric strains

Coupled modelling – Comparison Coarse mesh - Refined mesh

Coupled second gradient FE formulation

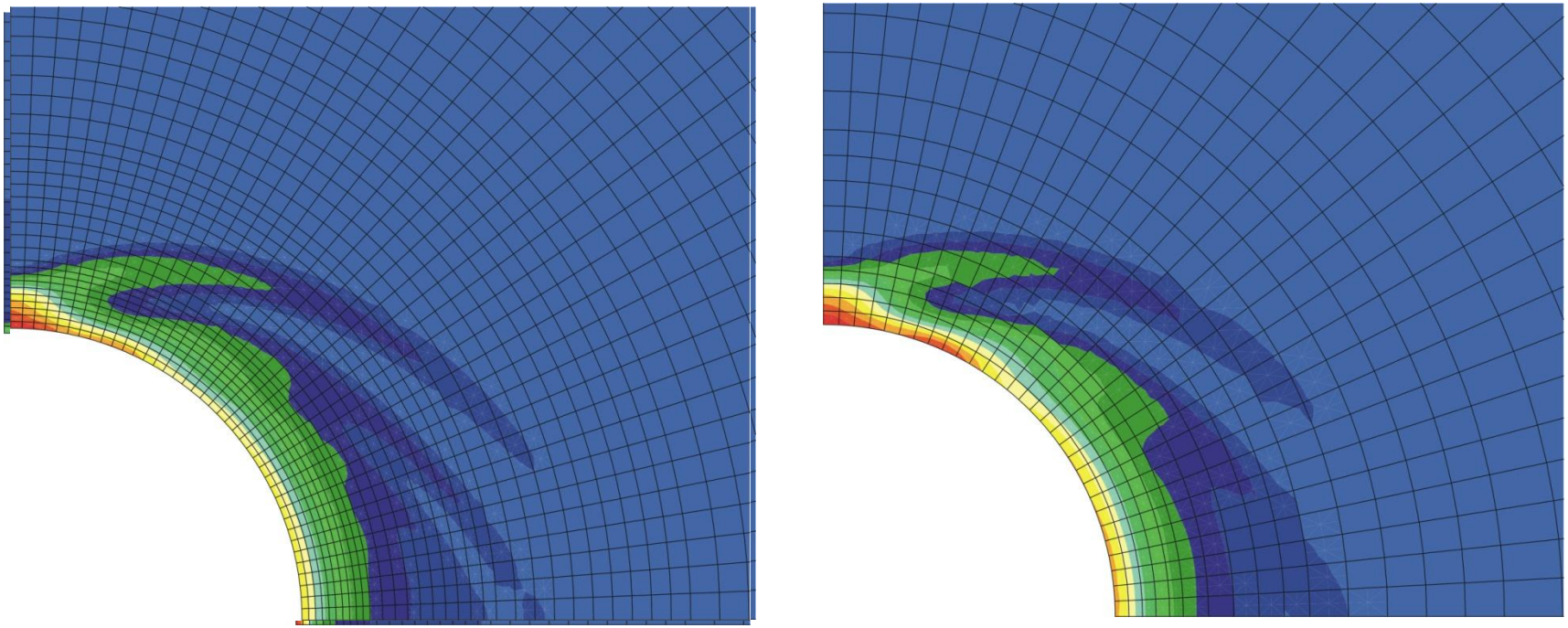

Deviatoric strains

Coupled modelling

Coupled second gradient FE formulation

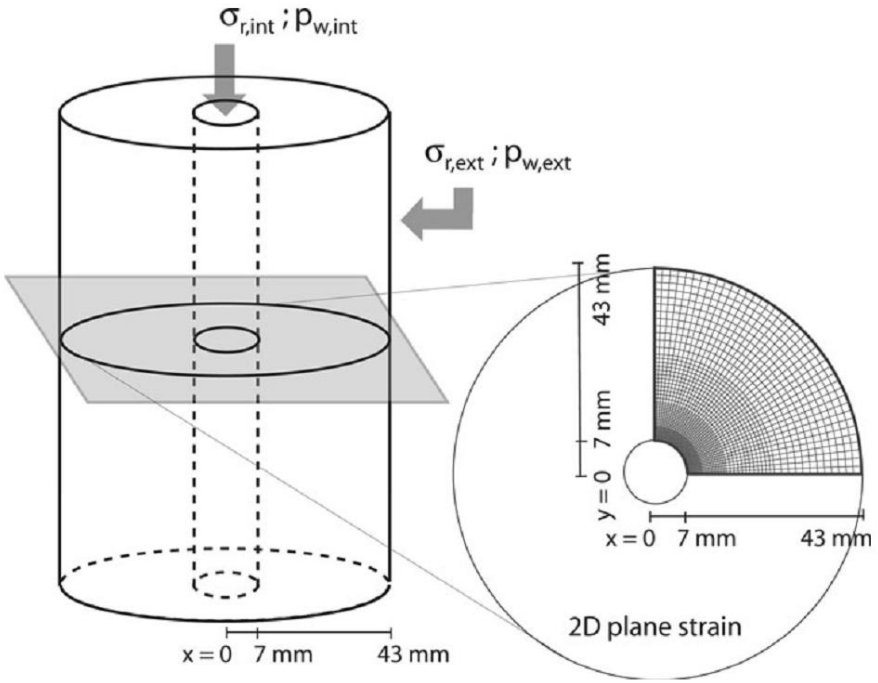

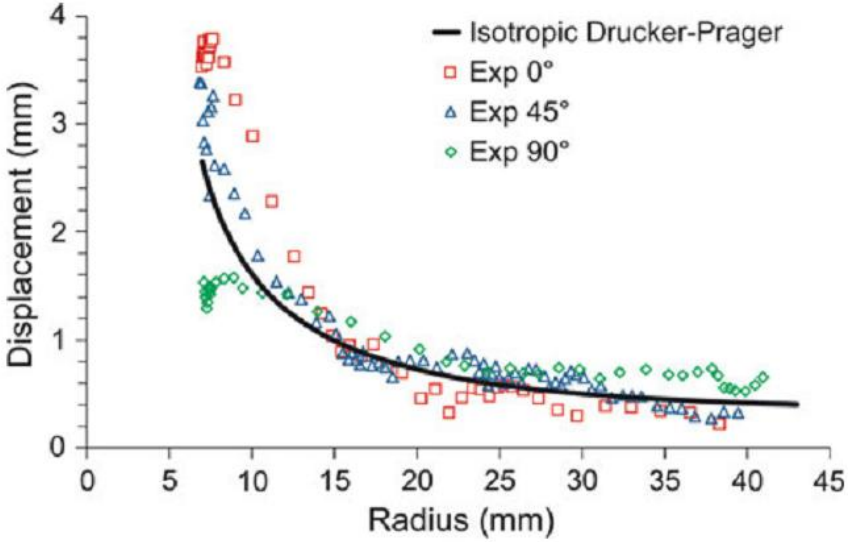

François et al., 2012

Coupled modelling

Coupled second gradient FE formulation

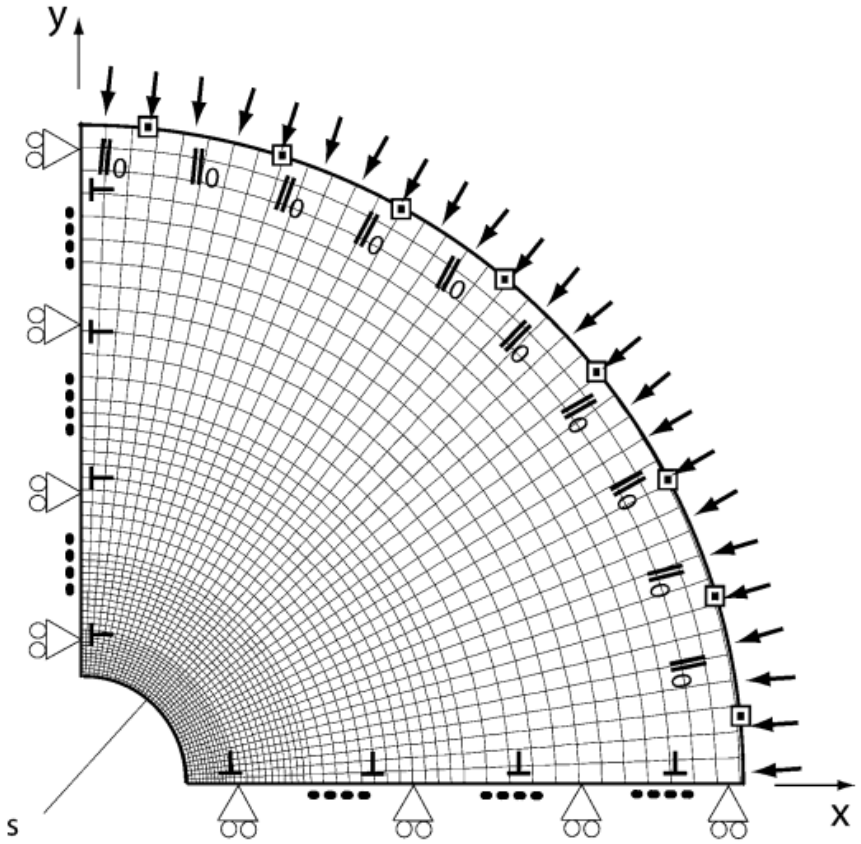

François et al., 2012

Coupled modelling

Coupled second gradient FE formulation

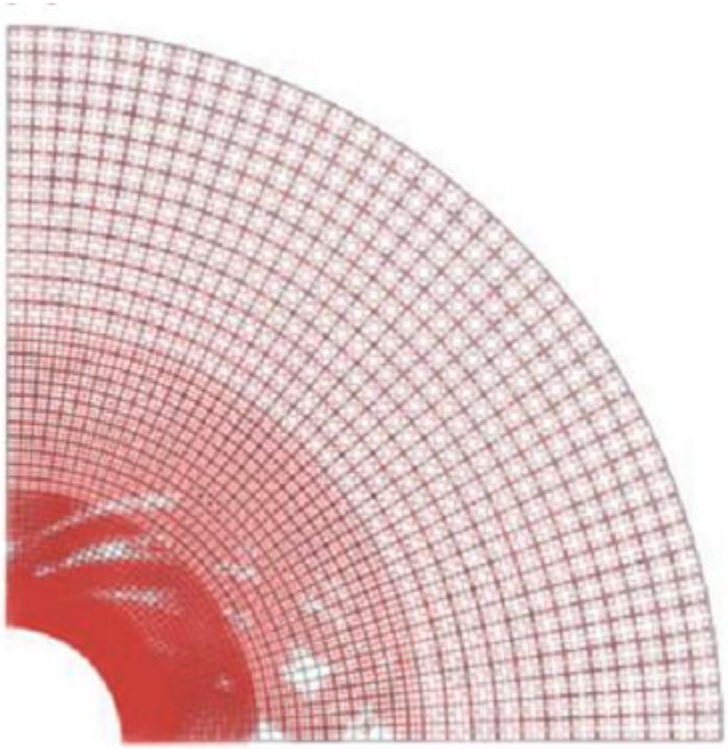

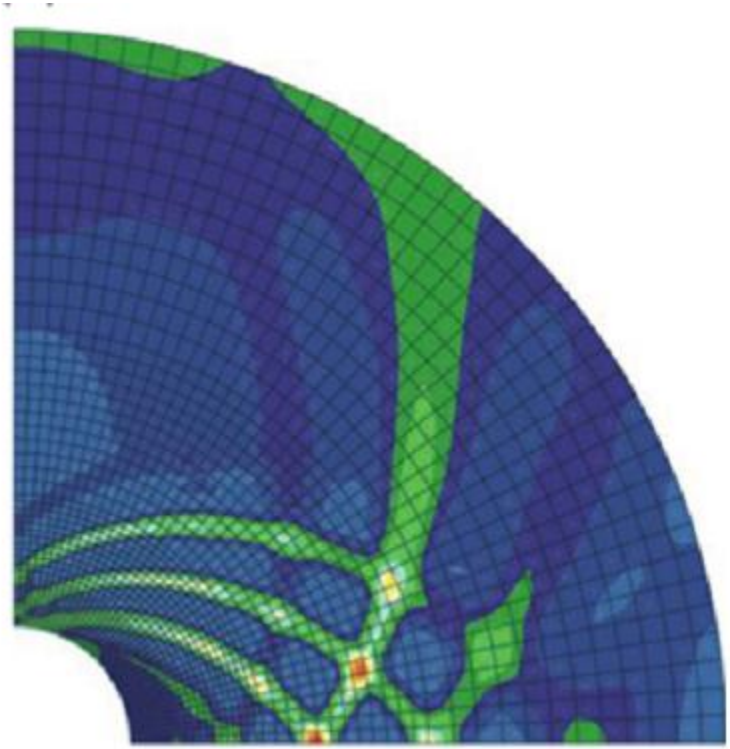

François et al., 2012

Coupled modelling

Coupled second gradient FE formulation

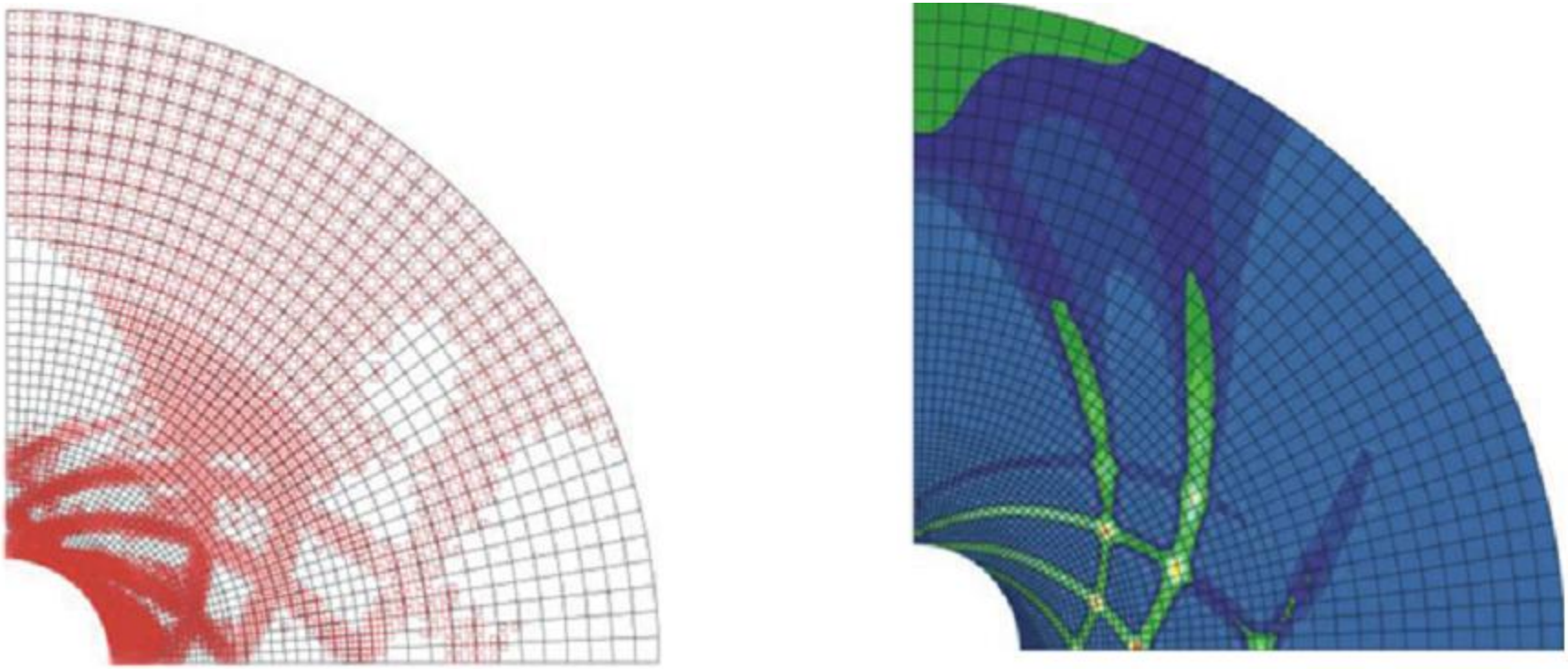

François et al., 2012

Coupled modelling

Coupled second gradient FE formulation

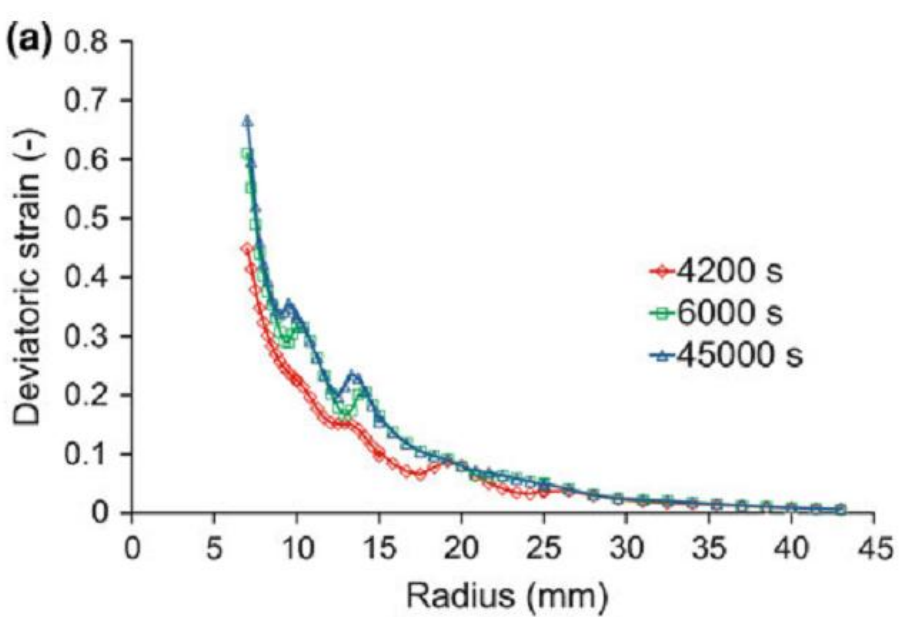

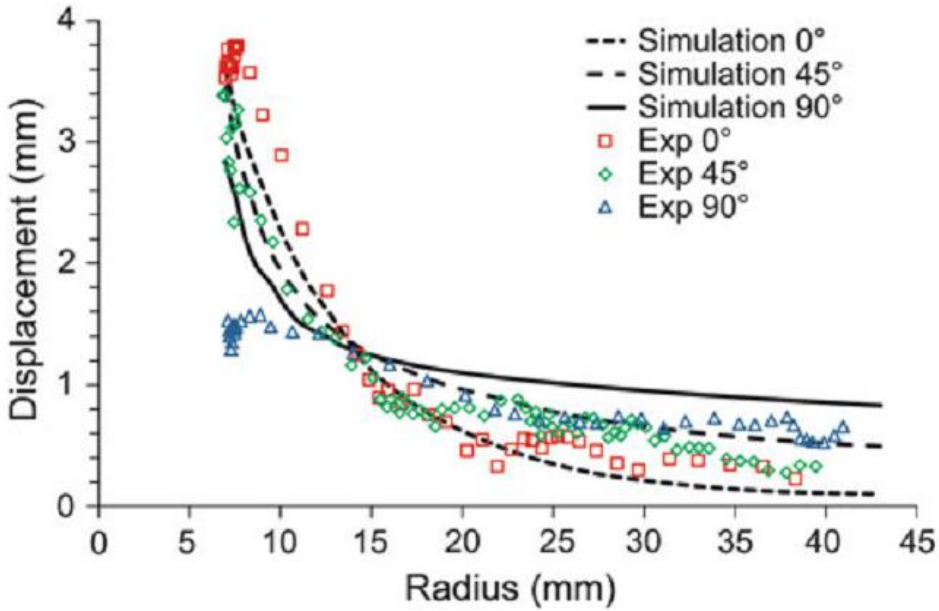

François et al., 2012

Outline:

- *Introduction*
- *Experimental observations*
- *Theoretical tools*
- *Numerical models*
- *Conclusions*

Strain localization in shear band mode can be observed in most laboratory tests leading to rupture in geomaterials.

Complex localization patterns may be the result of specific geometrical or loading conditions.

The numerical modelling of strain localization with classical FE is not adequate. Enhanced models are needed for a robust modelling of the post peak behaviour.

Many experimental works and numerical developments are necessary to improve the prediction of failure in boundary value problems